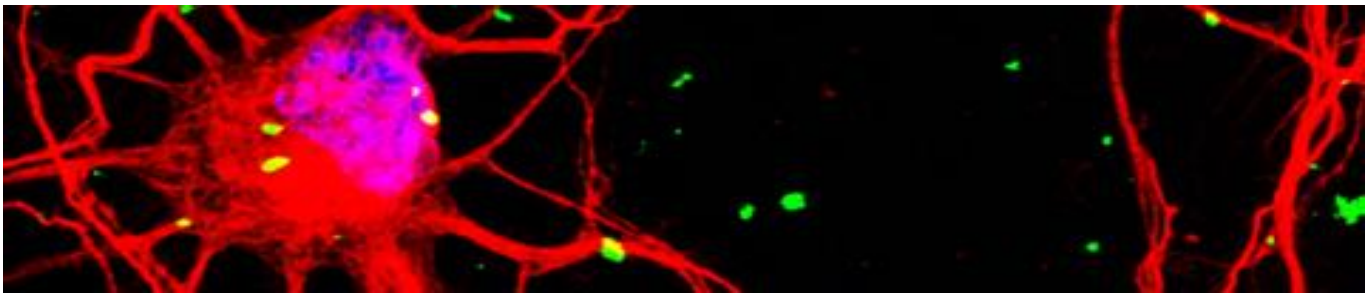

Corso di Dottorato in Neuroscienze
Curriculum Neuroscienze e Neurotecnologie
Ciclo XXXI

The octopus arm hydrostatic limb: an efficient link between form and function.

Author: Federica Maiole

Supervisor: Letizia Zullo, PhD

ISTITUTO ITALIANO DI TECNOLOGIA

UNIVERSITÀ DEGLI STUDI DI GENOVA

Index

1. Abstract

The *Octopus vulgaris* arm is a remarkable example of muscular hydrostat where extraordinary motor capabilities are achieved despite the absence of a rigid skeleton. The animal eight highly flexible arms exhibit a remarkable diversity and complexity of movements and can easily adapt to the surrounding environment. Indeed, unlike structures with rigid skeletal elements, whose movements are restricted to joints, in these arms, deformations such as bending, elongation, shortening, and twisting, can occur at any location and at multiple locations simultaneously. Furthermore, the octopus can vary the stiffness of its arms, transiently converting a flexible limb into a quasi-articulated structure to accomplish complex tasks like fetching objects and walking over the sea floor. For these reasons, for over a decades the octopus has been inspiring the design of flexible robotic arms and represents nowadays an "animal model" for soft robotics technologies.

The octopus behavior and locomotion are achieved through the combination of basic stereotyped arm motions. At the arm level, this can be obtained by the selective activation or co-activation of antagonistic muscles. The aim of this thesis is to elucidate the bases of octopus arm behavioural flexibility investigating the arm structure to function relationship. Here we show that, while having a morphologically continuous structure, the arm presents behaviourally relevant morpho-functional regionalization, especially evident at the arm apical region.

An additional level of flexibility in this system is achieved through the existence of transmural strain gradients generated by a decreasing waviness of elastic fibers from outer to the inner muscle layers determining a functional higher viscoelasticity of the outer muscle layers. This might be related with the distinct functions played by muscles during motions such as accommodation of strain of the inner muscle layers and storage and release elastic energy of the outer layers. This aspect might be important for the overall arm stabilization and compliance to deformation. In support of this data, we found differences in muscle activation properties wherefore inner layers behave as slow muscles and outer layers as fast muscles.
Moreover, differently from vertebrates, hydrostatic muscles can undergo large deformations thus changing dramatically the strain rate of each muscle participating in the motion. In this scenario, an activation pattern from a given motorneuron can find the same muscle in a very different strain rate during the motion. Here we found that muscle strain rate has indeed a profound influence on its mechanical work output and, in conjunction with the activation pattern and mechanism of E-C coupling, this feature might be exploited by the animal to produce a wide spectrum of arm motion.

Taken together these findings support the existence of a specific arrangement of highly coordinated muscles along and within the arm bulk that is consistent with the arm use.

This study is particularly relevant to further implementation in computational models able not only to simulate natural arm movements but also to predict, through a reverse engineering approach, the motion outcome of muscle ensembles. Moreover, conveying the principles governing arm flexibility might have an important impact into the design and fabrication of bio-inspired flexible robotic arms endowed with high compliance and adaptability.

2. General introduction

The octopus arm is a highly flexible appendage composed of mainly incompressible muscle tissue and lacking any rigid skeleton. This structure has been termed muscular hydrostat (Kier and Smith, 1985) for its isovolumetric structure where any dimensional change in one direction yields a variation in another direction. Several examples of muscular hydrostat exist in nature, among them cephalopod arms and tentacles, vertebrate tongues and the elephant trunk.

Muscle hydrostats represent a special class of muscles since they can work as motors to generate force for movements, or they can produce a variable stiffness to provide skeletal support. Stiffening of the octopus arm is especially interesting in view of the arm ability to control and modify rigidity at desired locations and in a relatively short time. This feature is fundamental to the production of a wide variety of complex motions ranging from swimming to crawling and fetching to end with articulated manipulation tasks.

Moreover, soft-bodies usually manifest a nonuniform distribution of circumferential strain during motions due to the position of the inner and outer muscles with respect to the induced deformation. In order to accommodate these strain differences, soft-organs manifest a specific organization of connective matrix that can generate potential transmural strain gradients. Connective tissue in muscle hydrostats plays critical roles in controlling shape and motions as it can provide structural reinforcement through stiffening, transmit stress and store elastic energy.

Hydrostatic muscles and the octopus arm in particular, currently represent an important source of inspiration in the field of bio-robotics and material science due to their interesting properties of softness, robustness, environmental adaptability and control mechanisms. In the last years, the development of the first bio-inspired soft robot prototypes paved the way for their implementation in society, human interaction and industry in spite of the classical rigid-bodied robots (Laschi and Cianchetti, 2014; Bao et al., 2018) (figure 1).

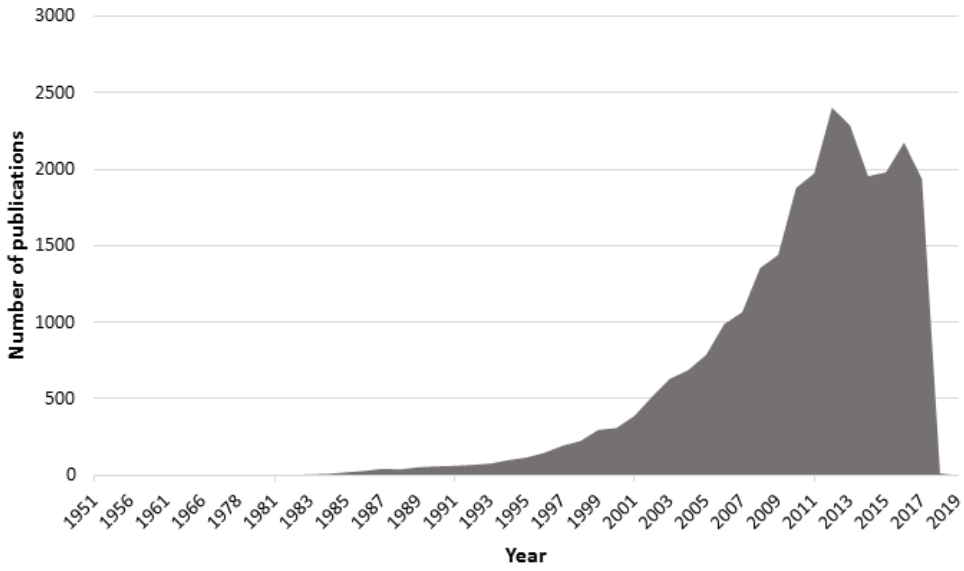

Figure 1: Trends in the number of published articles related to soft robotics by year.

Traditional rigid robots have the ability to perform a limited number of tasks that are mostly restricted by the robot size and shape. However, it will be advantageous in the future, that robots will be able to perform multifunctional tasks and adapt to a natural environment. Soft robots are expected to interact more safely with humans, to conform to a changing environment and to deal with dynamic tasks. Bio-inspiration provides an excellent example of how to build and control flexible structures and with respect to this, the octopus arm represents a one-of-a-kind model (Laschi et al., 2009; Cianchetti et al., 2015).

The aim of this thesis is to elucidate the structure-function relationship of the octopus arm hydrostatic muscle and to understand the mechanism by which this muscle reaches an optimal match between movement, coordination, energetic efficiency and functional demand. Understanding these morpho-physiological aspects will have an impact in the field of soft-robotics, where the development of soft-technologies, endowed with both adaptability and autonomous control, is still very challenging.

2.1 Structural organization of the octopus arm

2.1.1 Morphology of the octopus arm

The octopus arm is composed almost entirely of a tightly packed three-dimensional array of muscle fibers, surrounding a central axial nerve cord running throughout the arm (figure 2).

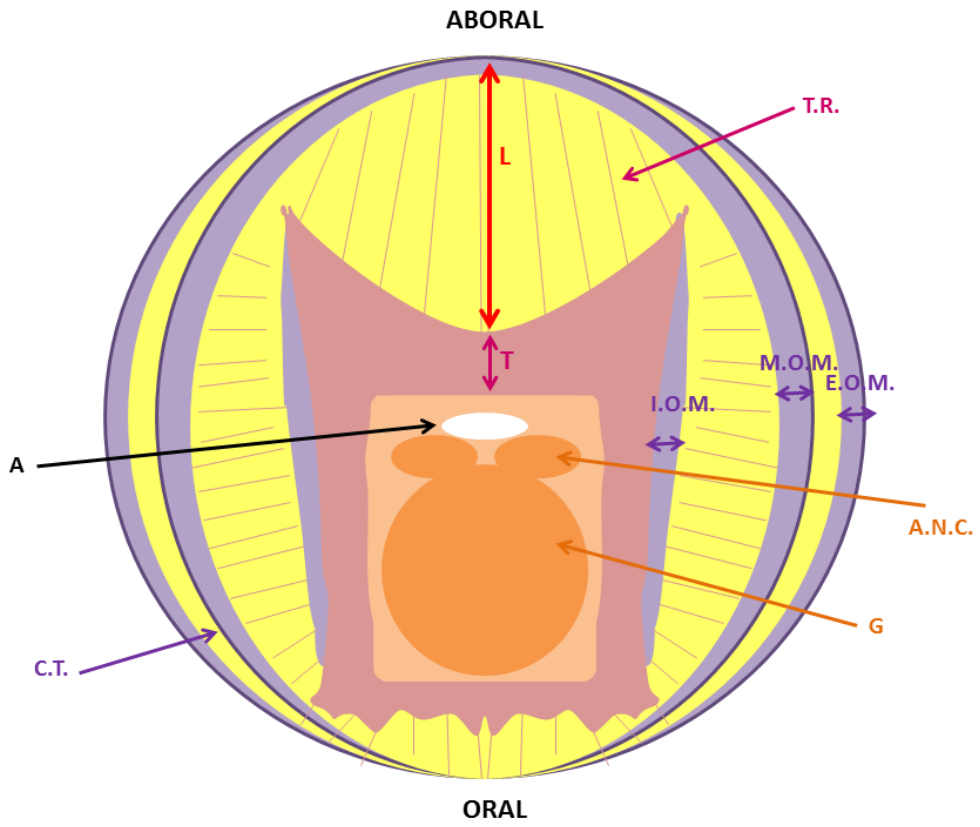

Figure 2: Transversal section of *Octopus vulgaris* arm. (*A: artery; A.N.C.: axial nerve cord; C.T.: connective tissue; G: ganglia; L: longitudinal muscles; E.O.M.: external oblique muscle; I.O.M.: internal oblique muscles; M.O.M.: medial oblique muscle; T: transversal muscles; T.R.: trabeculae.)*

Arm muscles are organized into transverse, longitudinal, and obliquely orientated groups. The transverse mass is the inner muscular portion of the arm bulk and it will be here referred also as inner muscle layer; it is located at the core of the arm and surrounds the axial nerve cord, the main constituent of the peripheral nervous system of the arm. Muscle fibers in the transverse muscle mass are orientated in multiple planes perpendicular to the longitudinal axis of the arm. They insert on connective tissue layers on the oral and aboral sides (figure 2) and transversely on connective tissues surrounding the oblique muscles. The transverse muscle fibers extending approximately parallel to the transversal plane originate on the thick crossed-fiber connective tissue sheets located on the oral and the aboral side of the arm and extend towards the central axis of the arm in longitudinal sheets between bundles of longitudinal muscle termed "trabeculae" (Graziadei, 1965).

The longitudinal muscle mass constitutes the main outer layer of the arm bulk and it will be here referred also as outer muscle layer; they are oriented parallel to the longitudinal axis of the arm and surround the central core of transverse muscle. The fibers extend longitudinally as bundles between the trabeculae of the transverse muscle mass.

The oblique muscles can be divided into external, medial and internal. The most superficial is a pair of external oblique muscle layers, occupying a lateral position and enclosing the remainder of the intrinsic musculature. A pair of median oblique muscle layers is located closer to the central axis of the arm. The internal oblique muscle layers are the most central and are located on each side of the central core of transverse musculature. The external and medial oblique muscles originate and insert on the oral and aboral connective tissue layers. A

thin layer of muscle fibers arranged circumferentially has also been described (Kier and Stella, 2007). This layer is thickest on the aboral side and covers the aboral crossed-fiber connective tissue layer. It extends down each side of the arm as a thin layer, wrapping the external oblique muscle layers, and then inserts on the oral crossed-fiber connective tissue layer.

At the single cell level, all arm muscles present the oblique striation typical of many cephalopod muscles that will be hereafter referred as striated muscles.

2.1.2 The structure of cephalopod myocytes

Cephalopod arm muscles differ from the typical skeletal muscles of vertebrate model species. Arm muscle fibers are mononucleated as opposed to several fused myofibers of vertebrate skeletal muscles (reviewed in Abmayr and Pavlath, 2012). They are small cells, generally not exceeding 8–20 μm in diameter and up to 1 mm in length, with a central mitochondrial core and a cortical zone occupied by mostly obliquely arranged myofilaments (figure 3a) (for a review see Zullo et al. 2017). At the microscopic level, molluscan muscles show the typical banding pattern of striated muscle, but the A- band, I- band and Z material are at a small angle (~ 6 to 12°) to the fiber axis, giving an oblique striation (figure 3b). The M-line is absent.

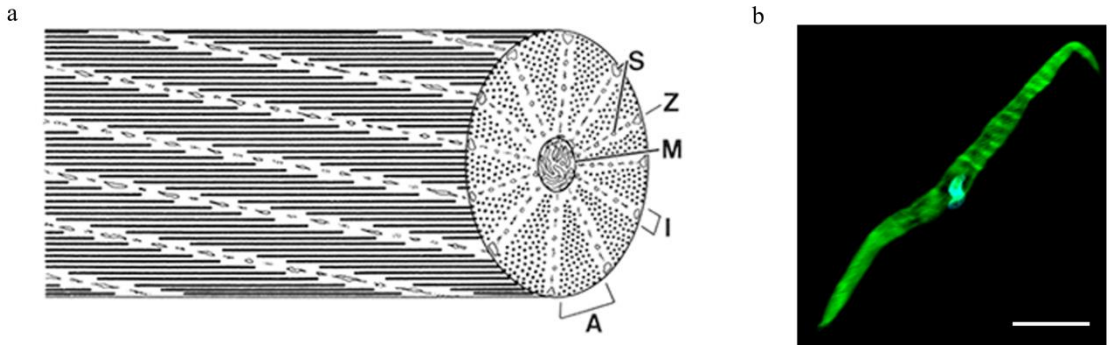

Figure 3: a) Muscle protein organization within the sarcomere of an obliquely striated muscle. A, A-band; I, I-band; M, mitochondria; S, sarcoplasmic reticulum; Z, elements

(from Kier, 1996). b) Single nucleus position and oblique striation are clearly visible in the imaged muscle fiber (DAPI, blue; phallacidin, green – scale bar: 50µm).

The sarcoplasmic reticulum is present in three zones: surrounding the mitochondrial core, scattered among Z material and adjacent to the sarcolemma, where it forms the subsarcolemmal cisternae, usually at the border of opposing cells (figure 4). At this location, it forms a complex with the membrane designated as a dyad, due to the similarities with the muscular vertebrate triad.

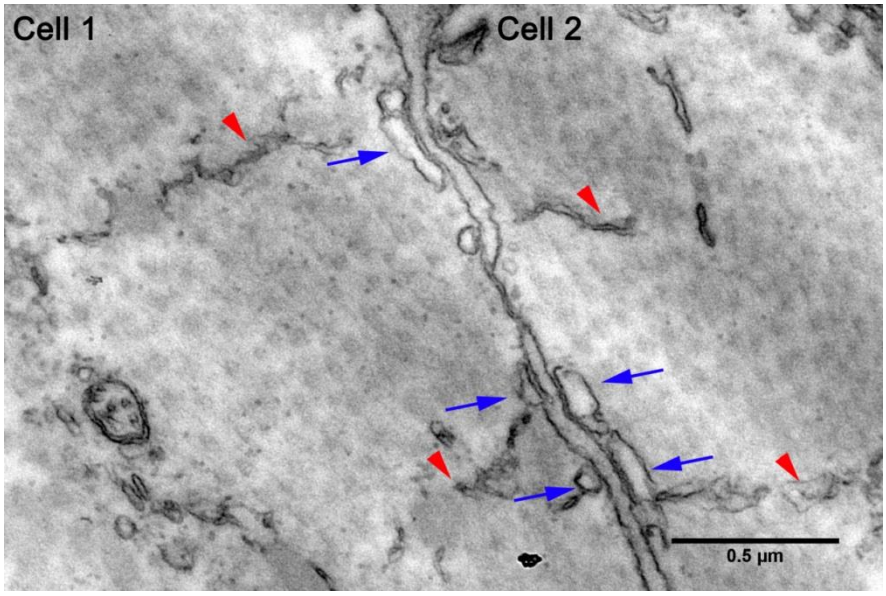

Figure 4: Electron micrograph of two facing myocytes in the transversal plane. Blue arrows point at subsarcolemmal cisternae. Red arrowheads point at Z lines.

Unlike vertebrates, cephalopods do not show significant differences in the proteins of the myofilament lattice in the various muscle groups. Six myosin heavy chain isoforms have been identified in *Octopus bimaculoides* muscles without any tissue-specific pattern of expression (Shaffer and Kier, 2012). Moreover, a thick filament core protein typical of invertebrates, the paramyosin, has been identified in cephalopod muscles. Its content varies depending on

tissues and correlates with the tension which the muscle can develop (Lowy et al., 1964), being the most abundant in catch muscles. Paramyosin protein structure consists of a dimer of α-helical coiled-coil that constitute the backbone of thick filaments (Hooper, Hobbs, and Thuma, 2008). Tropomyosin, instead, shows a low aminoacidic similarity with the human protein (Motoyama et al., 2006)

In summary, this suggests that although sharing the acto-myosin composition (figure 5) and putatively the sliding mechanisms with vertebrate skeletal muscles, the regulation of contraction might be different in cephalopod muscle cells.

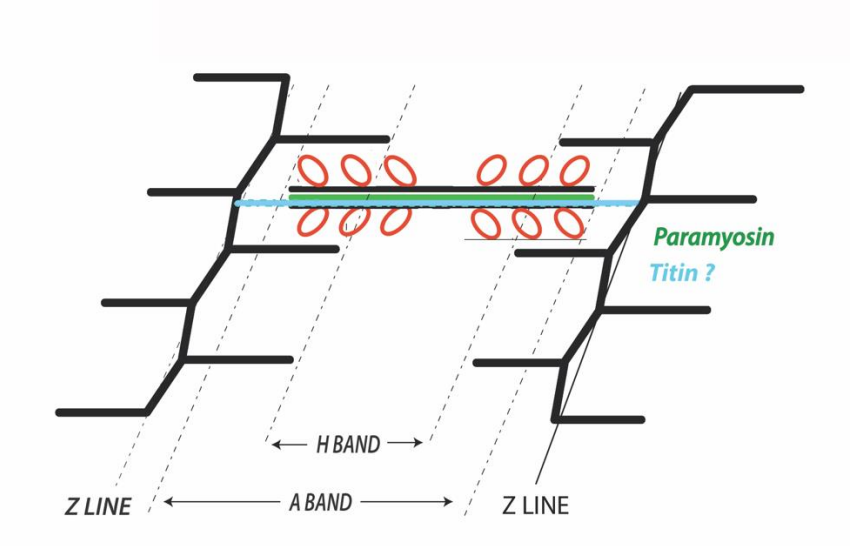

Figure 5: Octopus sarcomere structure. Myosin heads are shown in red (from Zullo 2017).

While at microscopic level muscles share the same structure, suggesting a similar mechanism for contraction, the difference in the dimensions and arrangement of muscle cells within each of the three muscle layers could be the keystone to understand their different performance during arm movement.

2.1.3 Connective tissue in cephalopod limbs

The nature of connective tissue of cephalopods is yet to be completely determined. As for mammalian, there is evidence of collagen heterogeneity. Two types of collagen, I and V, were

identified as the principal constituents of the connective tissue in various cephalopods: *Todaropsis eblanae*, *Illex coindetii*, *Loligo pealii*, *Sepia officinalis*, *Octopus vulgaris*, *Eledone cirrhosa* (Bairati et al., 2003; Corbetta et al., 2002; Morales et al., 2000).

The exact composition of the octopus arm connective tissue is unknown, although the presence of elastic components has been widely described in another kind of muscle hydrostat, the squid mantle muscles (Thompson et al., 2001; Kurth et al., 2014). In addition to the expected functional biomechanical influence, this aspect can also be particularly relevant when considering muscle energetics. Indeed, muscles can generate a different amount of power depending on the role they play in a certain behavior (absorbing or generating energy) and elastic elements function like springs that alternatively store and release elastic energy as animals move along thus reducing the metabolic cost of locomotion. This point has also been addressed in this work with the aim of understanding the molecular pathway involved during arm.

2.2 Muscle energetics and the control of Muscle Mass

Cephalopod muscle metabolism can be both aerobic and anaerobic. Differently from vertebrates, where lipids are the most important substrate during aerobic production of energy (Farrell et al., 2006), in cephalopods both the metabolisms are fueled by carbohydrates (Hochachka, 1983).

Interestingly, a metabolic differentiation into three zones of varying oxidative capacity has been found in the squid mantle mass (Mommsen et al., 1981), with a pattern of aerobic mitochondrion-rich cells at the inner and outer layer and anaerobic cells with a higher amount of glycolytic-cytosolic enzymes in the middle.

Muscles have an intrinsic potential to adapt to physiological stimuli, such as different exercise paradigms. This adaptation takes place by the integration of multiple signaling pathways that are able to control and modulate transcription factors and in turn protein synthesis and degradation. Relevant to this work, the effect of muscle exercise on one of the most conserved pathways (the mTOR pathway) involved in sensing of muscle cellular nutrition and energy status has been studied.

Anaerobic stimuli and mechanical overload promote muscle mass increase and fiber size. mTOR, in the form of its complex mTORC1, is the key regulator that has been implicated in the hypertrophy mechanisms following these stimuli (figure 6).

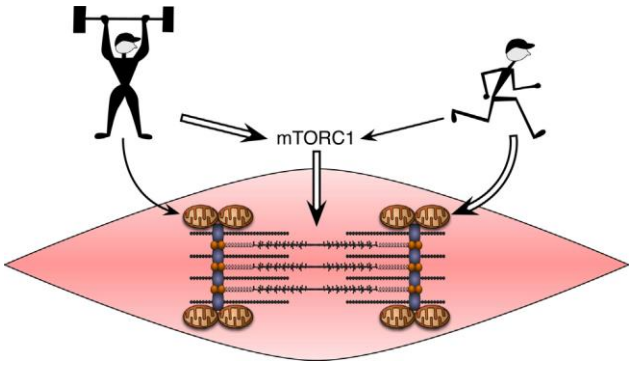

Figure 6: Cartoon representing the activation of mTOR signaling pathway by resistance exercise (from Watson and Baar, 2014).

mTOR is an evolutionary conserved serine/threonine kinase involved in sensing nutrient availability and energy status and regulates cell growth, survival, differentiation, autophagy, and metabolism (Laplante and Sabatini, 2012). mTOR assembles with other proteins forming two diverse complexes: mTORC1 and mTORC2. mTORC1 includes the regulatory associated protein of mTOR (raptor), the 40 kDa proline-rich Akt substrate (PRAS40), the DEP domain-containing mTOR-interacting protein (DEPTOR), and the mammalian lethal with SEC13

protein 8 (mLST8). mTORC1 is inhibited by rapamycin and its activation depends on growth factors, genotoxic stress, energy status, oxygen, and amino acids.

mTORC1 has two downstream targets: it phosphorylates p70S6k and 4E-BP (figure 7). Activated p70S6 kinase phosphorylates its target substrate S6, a ribosomal protein, whose activation enhances protein synthesis. The phosphorylation of the eukaryotic translation initiation factor 4E -binding protein (4E-BP) breaks the binding to eIF4E that can initiate cap-dependent translation.

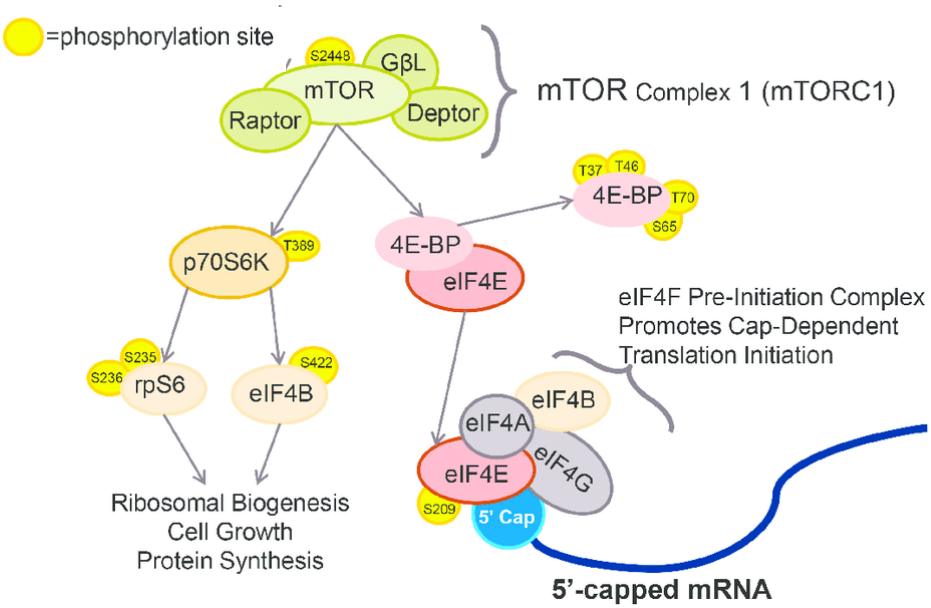

Figure 7: mTOR pathway. Adapted from Beckham 2016.

The overall effect of this process is the modulation over time of the muscle responses to motorneurons inputs that, in turn, are activated from the higher motor system of the central brain mass (Zullo et al., submitted).

2.3 Transmission and coupling of arm muscles

Motoneuron signal transmission in the octopus arm is exclusively excitatory and mainly based on cholinergic innervation. Differently from vertebrate, octopus myofibers are not

multiterminally innervated (figure 8a and b) and have a high input resistance. This causes the cell to be isopotential, therefore, each synaptic input can control the membrane potential of the entire cell via a single localized synaptic junction (figure 8b) (Bone et al., 1995; Matzner et al., 2000; Feinstein et al., 2011).

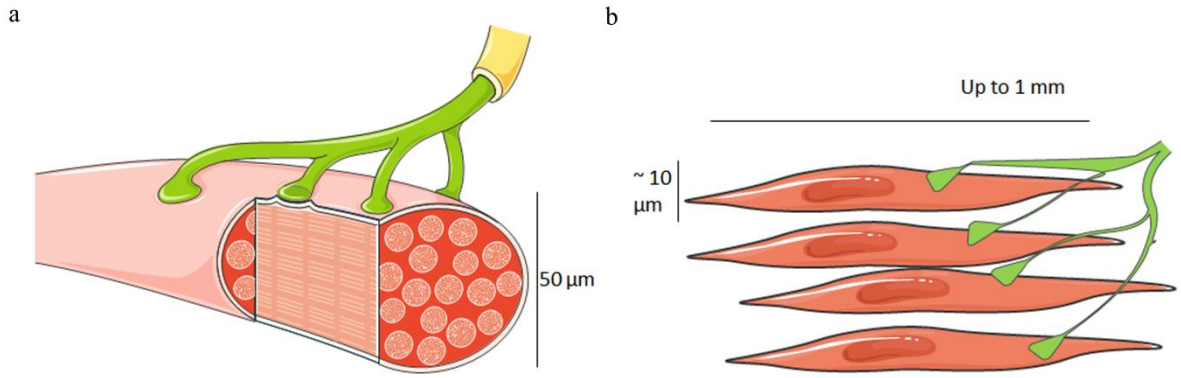

Figure 8: Vertebrate (a) and octopus (b) muscle innervation

Differently from vertebrates, action potential in cephalopod striated muscles is based on the activation of voltage-gated L-type Ca^{2+} channels that induce a massive entrance of Ca^{2+} from the extracellular space (Rokni and Hochner, 2014). Although excitation-contraction coupling in cephalopod is mainly triggered by extracellular calcium influx (Bone et al., 1995), internal stored Ca^{2+} release from the sarcoplasmic reticulum (SR) may be important to finely regulate arm movement.

As shown in figure 9, in skeletal muscles this release is mediated by the interaction between the voltage-gated Ca^{2+} channels, dihydropyridine receptors (DHPR), located on the sarcolemma, and the ryanodine receptors (RyR), located on the SR. In this configuration, DHPR and RyR are mechanically coupled and the sarcolemma depolarization induces conformational changes of DHPR that, in turn, triggers the Ca^{2+} release through RyR (figure 9a). In cardiac muscle, sarcolemma depolarization opens the DHPR thus allowing the influx of external Ca^{2+}, which triggers Ca^{2+}-induced Ca^{2+} release from the SR.

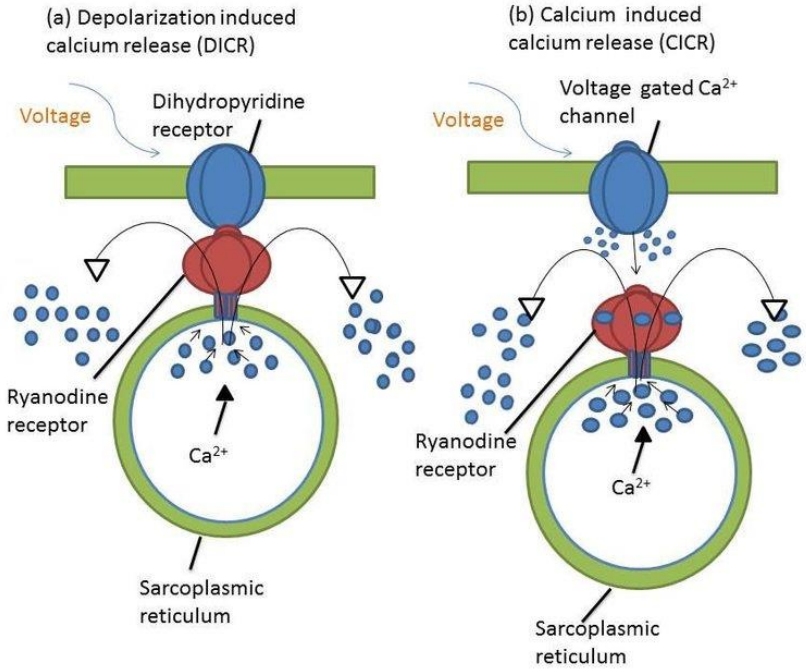

Figure 9: Vertebrate skeletal and cardiac muscle model of excitation-contraction coupling (adapted from Lodish 2000)

The presence of DHPR and RyR in cephalopod muscles and their possible involvement in muscle activity has not yet been clarified and, due to its importance in the dynamic of muscle contraction, it has been investigated more in detail in this work.

2.4 Coordination of muscle ensembles: the presence of gap junctions

The high coordination in cephalopod limb mobility is achieved despite each myofiber is monosynaptically innervated. The physiological mechanisms underlying this fine coordination are still debated but insights might come from studies of *Caenorhabditis elegans* somatic musculature that shows a high morphological affinity with that of the octopus arm. Indeed, in *C. elegans* muscles are obliquely striated with respect to the longitudinal axis of the muscle cell. Furthermore, muscle cells are unfused and uninucleated, with no vertebrate equivalent T-tubule system, and, as for octopus, they rely on Ca^{2+} entry through voltage-activated L-type Ca^{2+} channels across the muscle plasma membrane to initiate muscle contraction (Wood, 1988; Raymond et al., 1997; Jospin et al., 2002). Moreover, it has been suggested that the SR is nonessential for the excitation-contraction but might be relevant to other features, such as to enhance and orchestrate the animal body motility (Norman and Maricq, 2007). In particular, it has been shown that in *C. elegans* active functioning gap junctions can synchronize action potentials and Ca^{2+} transients in the body wall muscles (Liu et al., 2006; Liu et al., 2011).

Invertebrate gap junctions are formed by innexin, a family of protein analog to vertebrate connexin (Norman and Maricq, 2007). Innexins consist of four transmembrane helices, two extracellular loops, and N and C termini located at the cytoplasmic side. Two cysteine residues in the extracellular loops and YYQWV amino acid in the transmembrane domain are present and conserved among all invertebrate innexin (Bauer et al., 2005). In vertebrates, the hexamers of connexin or pannexin proteins constitute the hemichannels and in invertebrates, the innexins are also believed to form hexameric channels (Oshima et al., 2013) (figure 10).

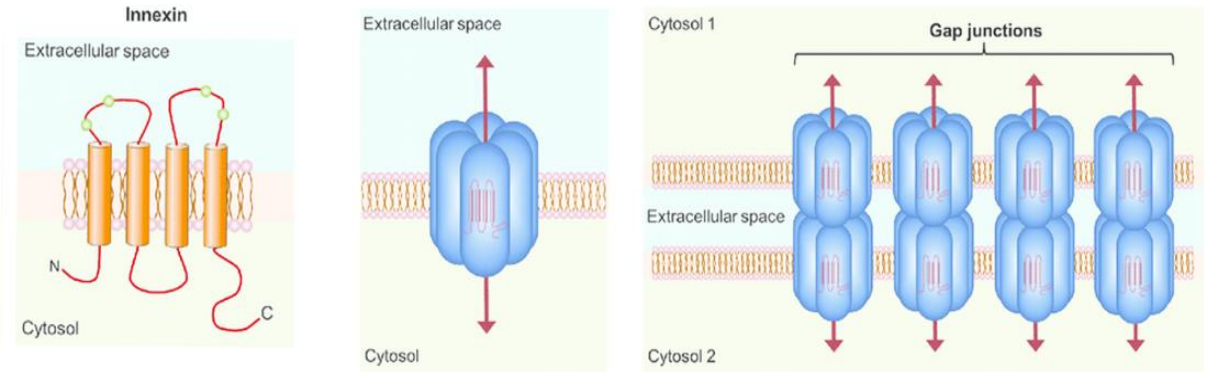

Figure 10: Innexin channel structure (adapted from Gajardo-Gómez et al, 2016)

The *C. elegans* genome encodes 25 innexin genes, and it has been shown that every cell type expresses one or multiple different innexin genes (Altun et al., 2009). Gap junctions typical of its body wall muscle are composed by innexin unc-9 oligomers forming a hemichannel. The assembling of two hemichannels from neighbor cells yields to a functional channel, which allows a bidirectional electrical and metabolic signaling.

Given the affinity with *C. elegans* somatic musculature, the coordination of muscle ensembles in the octopus arm might be similarly achieved through physiologically active gap junctions (for a review see Zullo et al., 2017).

3. Materials and methods

3.1 Animal treatment

Specimens of *O. vulgaris* of both sexes were collected from local anglers of the Ligurian coast. Animal experimentations comply with the indications reported in the European Directive 86/609/EEC and were approved by the Institutional Review Board and by the Italian Ministry of Health (authorization n. 1111/2016-PR and 465/2017-PR).

Following captures, the animals were placed in 80x50x45 cm marine aquarium tanks filled with artificially prepared sea water (SW, Tropic Marine) and kept at a temperature of 17°C at 12h light/dark cycle. Octopus environments were enriched with sand substrate and clay pot dens. Water cleaning and oxygenation were assured by a pump-filter and aeration system which continuously circulated the water through biological filters; all relevant chemo/physical water parameters were checked daily. Animals were left to adapt to captivity for at least 5 days before experimentation. Octopuses were inspected daily and fed with shrimps 3 times per week.

For histological, biomolecular and biochemical experiments, animals were anesthetized in ethanol 2% (v/v) in SW and samples of interest were collected. For biophysical investigations, animals were anesthetized in 3.5% $MgCl_2$ in SW, since ethanol exposure induced muscle stiffness. A short segment was then cut from the middle-end of the arm and moved to oxygenated cold SW. The animals were immediately moved back to their own tank and a mantle massage was performed to help respiration rescue. Recovery was monitored inspecting animal behavior.

3.2 Histology

Arms ranging from 35 to 38 cm in length were employed. Samples were dissected at various locations along the arm thus providing basal (B, ~ 6 cm from the arm base), central (C, ~16 cm from the arm base) and apical (A, toward the arm end tip) portions as shown in figure 11 (see Fossati et al. 2011).

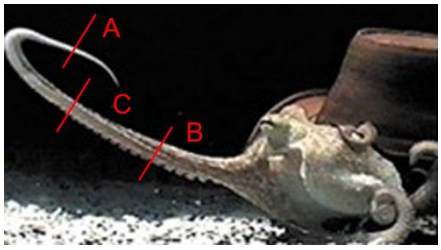

Figure 11: Octopus arm segment identification. (A: apical; B: basal; C: central)

Arm samples were fixed overnight in 4% Paraformaldehyde in artificial sea water (ASW: NaCl 460mM, KCl l10 mM, $MgCl_2$ 55mM, $CaCl_2$ 11mM, Hepes 10mM, glucose 10mM - pH 7.6) and cryopreserved in 30% sucrose in PBS overnight or until sunk. Tissues were then embedded in OCT compound, serially sectioned on a cryostat at 10-25µm and collected on Super frost slides (Bio-optica).

These sections were then processed using the standard Nissl staining to identify different muscle layers and perform further morphometric analysis.

Picrosirius red staining (Bio-optica) was performed on longitudinal and transverse arm sections to visualize collagen distribution and organization in longitudinal and transverse muscle.

3.3 Morphometrics

Anatomical descriptions of arm muscle organization was performed on Nissl stained transverse sections of B, C and A samples (defined in figure 11) by measuring the dimensions of the following muscles (see figure 12): aboral longitudinal muscle (L.A); lateral longitudinal muscle (L.L.); oral longitudinal muscle (L.O.); internal oblique muscle (I.O.M.); medial oblique muscle (M.O.M.); aboral transverse muscle (T.A.); transverse insertion (T.I.); lateral transverse muscle (T.L.); oral transverse muscle (T.O.).

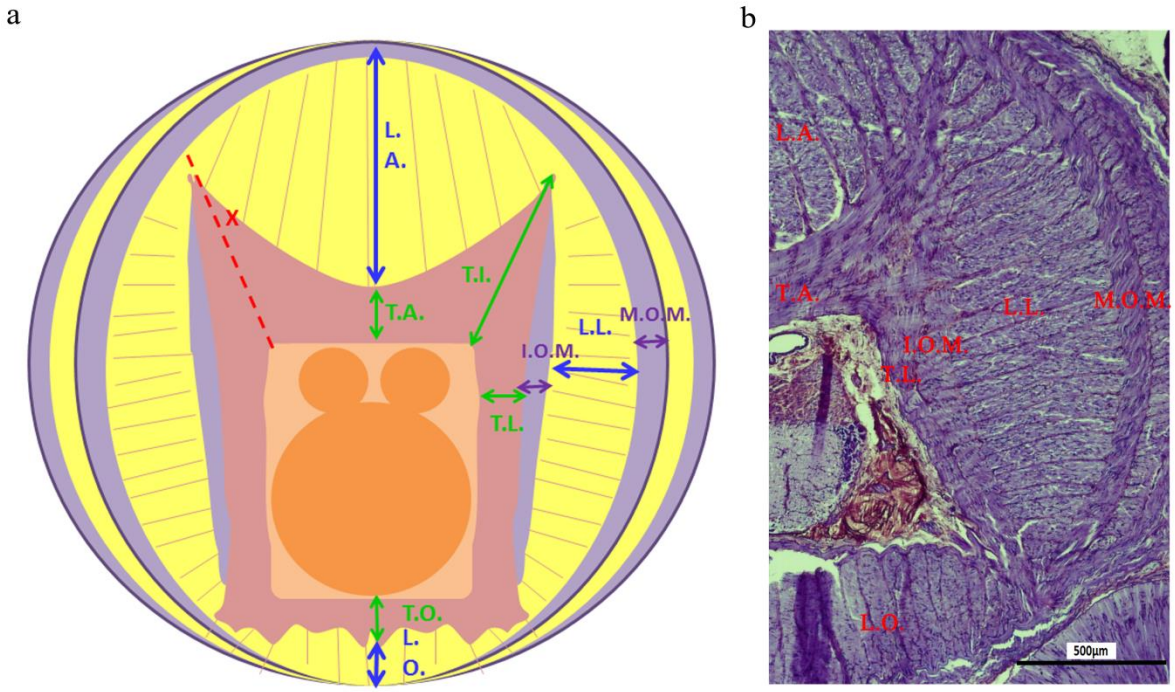

Figure 12: a) Scheme representing the measure taken on transverse section. (L.A.: Aboral longitudinal muscle; L.L.: Lateral longitudinal muscle; L.O.: Oral longitudinal muscle; I.O.M.: Internal oblique muscle; M.O.M.: Medial oblique muscle; T.A.: Aboral transverse muscle; T.I. Transverse insertion; T.L. Lateral transverse muscle; T.O.: Oral transverse muscle; X: reference length for T.I. measurement). b) Nissl staining on transverse section of the central segment of the arm.

Morphometry of elastic components was performed by measuring the orientation and level of coiling of elastic fibers within longitudinal and transverse muscles and expressed respectively by mean of two indicators: the chaos index (C.I.) and the waviness index (W.I.).

C.I. was defined as the angle between the elastic fiber main axis and the longitudinal axis of muscle cells (figure 13). A chaos index of 90° indicates that elastic fibers are oriented perpendicularly to the main muscle force direction, while at 0° elastic fibers are parallel to the muscle fiber main axis.

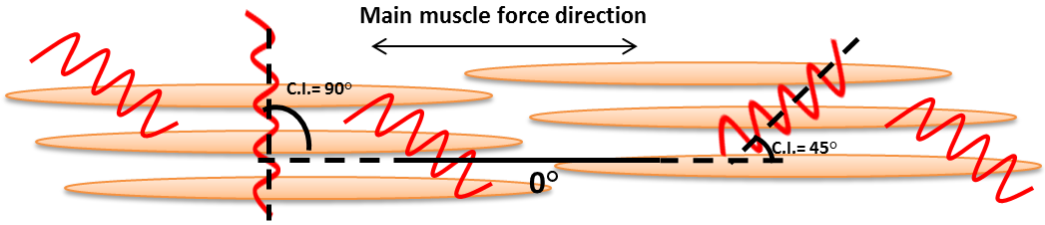

Figure 13: Scheme representing the chaos index analysis. Muscle fibers are represented in pink and elastic fibers in red (C.I.: chaos index).

Quantification of the coiling of elastic fibers was performed according to the method proposed by Kurth. In detail, the ratio between the total length of the folded fiber and its end-to-end straight-line distance (Kurth et al., 2014). Thus, a W.I. of 1.0 corresponds to a straight (non-coiled) fiber and higher values to increase in coiling (figure 14).

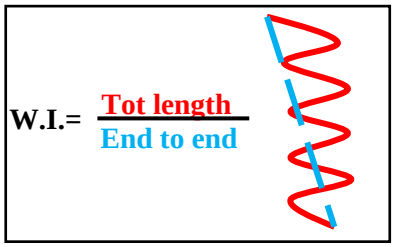

Figure 14: W.I. analysis. (Red line represents the elastic fiber total length; light blue is the end to end fiber length)

3.4 Muscle mechanics

3.4.1 Experimental setup

The active and passive properties of octopus arm muscles were investigated on *in vitro* preparations using a system composed by a Dual-Mode Lever Arm System (Aurora Scientific – 300C-LR) mounted on a muscle test chamber with integrated stimulating electrodes (Aurora Scientific – 801C) schematized in figure 15. A current-voltage bi-phase stimulator (Aurora Scientific – 701B) and a LabVIEW based Data Acquisition and Analysis System (Aurora Scientific – 604A and 605A) were employed. This complete system is able to control and measure both length and force within a range of 0 - 1.0 N and has a length excursion of 10 mm. Data were acquired at a sampling frequency of 10kHz and bandwidth filtered at 10Hz - 3.3kHz.

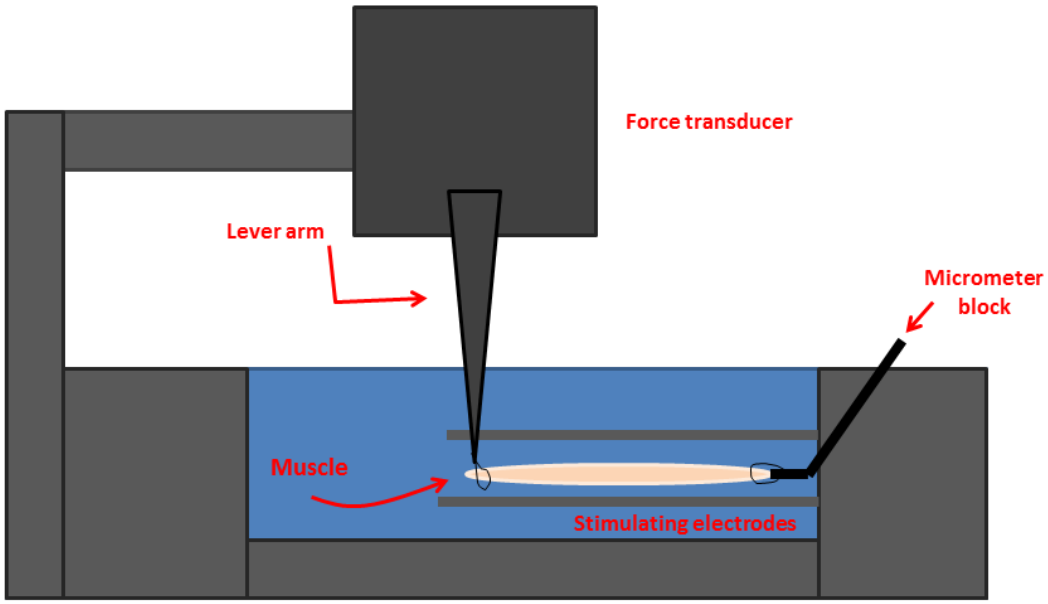

Figure 15: Schematic representation of the Dual-Mode Lever Arm System

3.4.2 Muscle preparations

Bundles of fibers from longitudinal and aboral transverse muscles were employed for biomechanical experiments. Bundles ranging from 5-8 mm of length and 2-5 mm width were dissected under a stereo microscope at 4°C in ASW. Muscle preparations were attached with suture thread to the micrometer block on one end and to the lever arm on the other and assured with double square knots. Preparations, placed in the *in vitro* bath, were continuously superfused with oxygenated ASW at 16 °C using a peristaltic pump (SJ-1220, Atto Co. - volume exchange rate 12mL/h). Figure 16 shows a typical dissection of longitudinal (a, b) and transverse (a, c) muscles.

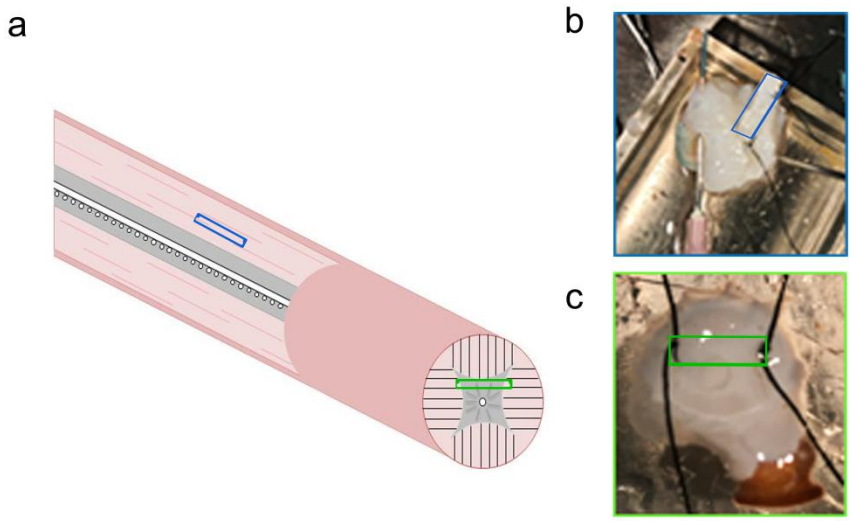

Figure 16: a) Graphic representation of muscle bundle preparations. (Blue: Longitudinal; Green: Transverse); b) Longitudinal and – c) transverse muscle strip dissections

Transverse muscle fibers were attached so that knots position allowed the exclusive measurement of their force-length changes (Kier and Curtin, 2002). Once positioned into the bath, the muscles were allowed 3 minutes rest. Thereafter, resting tension was set as 0g and the muscle length in this position, defined as initial length (L_0), was measured.

Due to their morphological differences, the cross-sectional area (CSA) was measured with two distinct formula for longitudinal and transverse preparations. Longitudinal muscle preparations were assumed as cylindrical shaped:

$$CSA_{long} = \pi r^2$$

where *r* is half of the diameter.

Transverse muscle preparations were assumed as parallelepiped-shaped:

$$CSA_{trans} = HW$$

where *H* is the height and *W* is the width of the sample.

3.4.3 Protocols

To study the muscle biomechanics and to dissect muscle active and passive components, the three elements Hill model was used as a framework (Hill, 1938) (figure 17).

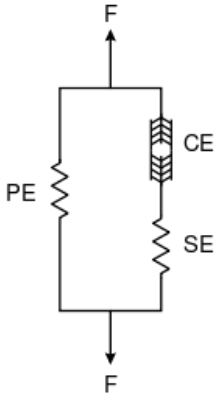

Figure 17: Hill model. (CE: contractile element; PE: parallel elastic component; SE: series elastic component; F: force)

This model takes into account three components: the contractile element (CE), and two spring elements PE and SE, arranged in parallel and series with the CE respectively. During muscle contraction, CE force is developed through the formation of acto-myosin cross-bridges at the sarcomere level. Spring elements generate passive

forces and, in a typical vertebrate muscle, PE represents the elasticity of the connective tissue surrounding the contractile elements and SE represents the tendon and intrinsic elasticity of myofibers. Parallel and elastic elements can have a different stiffness (K) which characterizes their response to deformations.

3.4.3.1 Passive muscle properties

The **stress-strain profiles** of longitudinal and transverse muscles were investigated applying a step-stretch protocol up to 30% of the muscle L_0.

Force developed during isometric stretch was measured at the peak (figure 18a, grey shadowed region) and at the plateau phase (figure 18b, gray shadowed region) representing respectively the series elastic element force (F_{SE}) and the parallel elastic element force (F_{PE}) (see also figure 18).

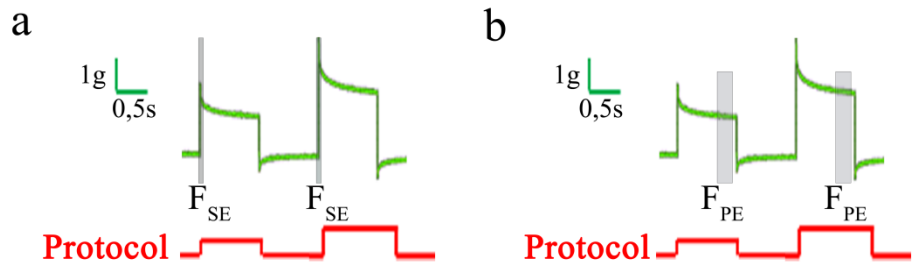

Figure 18: Exemplary traces of a step-stretch protocol (red) and force response (green). Shadowed regions represent the peak-force (a) for series elastic elements (F_{SE}) and the plateau-force (b) for parallel elastic elements (F_{PE}).

Stress (σ) was defined as the tension (F) per cross-sectional area (A):

$$\sigma = \frac{F}{A}$$

the Young Module (E) as a function of the strain (ε) was defined as the numerically approximated gradient of the stress-strain curve:

$$E = \frac{\Delta\sigma}{\Delta\varepsilon} = \frac{\sigma_{i+1}-\sigma_i}{\varepsilon_{i+1}-\varepsilon_i}$$

As the stiffness depends also on the physical dimensions of samples, its values were reported as:

$$K = \frac{EA}{L}$$

where L is the length of the sample and A its cross-sectional area. Stiffness was calculated for series elastic elements (K_{SE}) and for parallel elastic elements (K_{PE}).

The **hysteresis** behavior of longitudinal and transverse muscles was also investigated. A stress/strain protocol consisting of 4 cycles of 2.5Hz sinusoidal length changes of ±30% L_0 was employed (figure 19a). The third and fourth cycles of extension were analyzed. Muscle hysteresis percentage was calculated as

$$H = \frac{Ed}{Ei} \times 100$$

where E*d* is the strain energy dissipated and E*i* the strain energy input within each cycle (figure 19b).

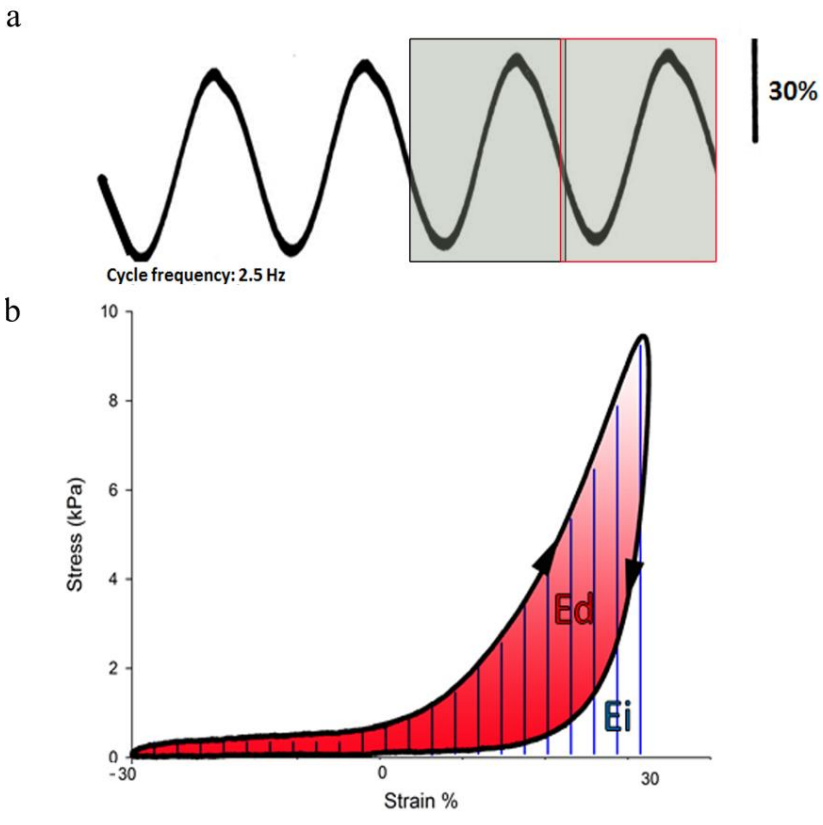

Figure 19: Hysteresis loop protocol. a) Sinusoidal length changes, cycles analyzed are highlighted in grey. b) Exemplary hysteresis loop from a stress-strain protocol from -30 to 30 strain %. The strain energy dissipated (E*d*) is represented by the area within the loop (in red) and the strain energy input (E*i*) by vertical line fill.

3.4.3.2 Active muscle properties

Isometric protocols

Muscle **twitch kinetics** were investigated stimulating preparations at 1A (pulse width: 0.2ms) and determining the following parameters, shown in figure 20: time to peak of tension (TPT; s), half relaxation time (1/2 RT; s), the maximum rate of isometric contraction per cross-sectional area (dP; g/(s·mm^2)) and the maximum rate of isometric relaxation (-dP; g/(s·mm^2)).

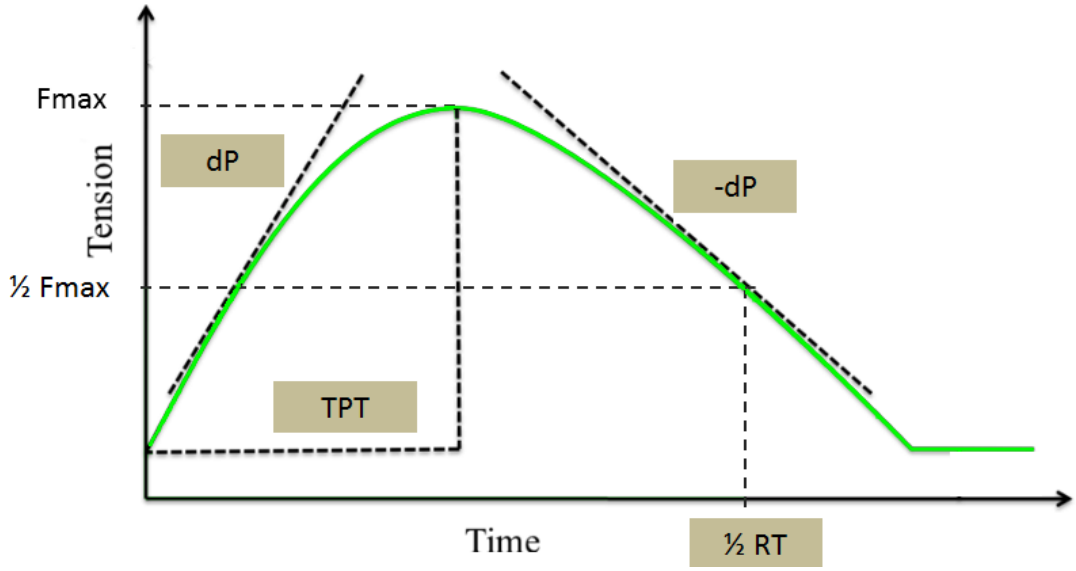

Figure 20: Muscle twitch kinetics properties (adapted from Pinotti et al., 2015). (TPT: time to peak of tension; dP: maximum rate of contraction; 1/2 RT: half relaxation time; -dP: maximum rate of relaxation).

To investigate the **length-tension** relationship, the force produced at different muscle lengths has been measured to determine the optimum length (L_{opt}) of the muscle corresponding to the length at which the maximum isometric force is developed. Samples undergoing step-stretch have been twitch stimulated (pulse width: 2ms, 1A) until the maximum active force was reached.

The **force-frequency** relationship has been studied with isometric protocols increasing the stimulation frequency from 10 to 100 Hz (pulse width: 0.5ms; train duration: 0.8s, stimulation amplitude: 1A). Muscles were allowed 5 minutes rest between successive stimuli. The peak force generated during each session was measured.

In order to perform **work loop** experiments, muscles underwent cyclic sinusoidal length changes while train stimulation at 1A (pulse width: 0.2ms; train frequency: 100Hz; train duration: 0.05s) was given at a specific time point (T) with respect to the length change cycle.

In details, 4 cycles of 0.5Hz sinusoidal length changes of ±2% L_0 were applied to longitudinal and transverse muscles while stimulated at 0, 25, 50 and 75% of the cycle (figure 21).

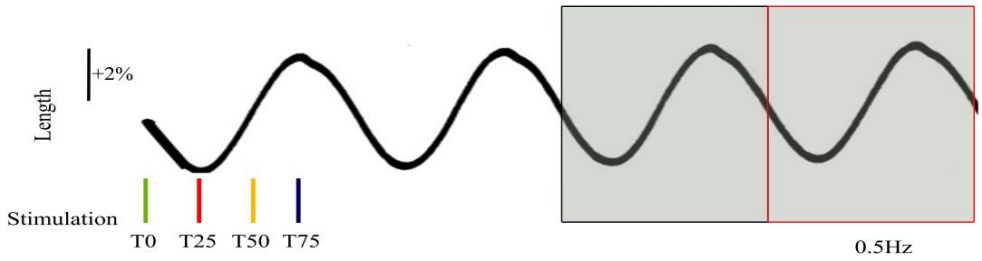

Figure 21: Protocol to determine the work loop representing the imposed cyclic sinusoidal length change (black) (frequency 0.5Hz, amplitude ±2%) and the stimulation time points (T0, T25, T50, T75). Cycles analyzed are highlighted in grey.

As previously described, clockwise direction of the loop is defined as negative work, indicating energy absorption, while counter-clockwise direction as a positive work output, representing the energy produced by the muscle. The net mechanical work produced has been calculated as:

$$Net\ work = Positive\ work - Negative\ work$$

Muscle uncoupling protocol

Isometric protocols were also employed to study the effect of 2-Octanol (Sigma Aldrich), a gap junction blocker, on muscle contraction. Muscle contraction in control condition was first assessed with twitch stimulation (0.2ms; 1A) every 3 minutes to determine basal muscle force production. Bath perfusion was then stopped and Octanol was added to the bath to a final concentration of 2.5mM. Muscle force production was then measured at a regular interval of 3 minutes until no residual force was detectable (figure 22).

Figure 22: Muscle uncoupling protocol.

Isotonic protocol

Muscle **force-velocity** has been determined using an isotonic protocol. As a first step, the maximum active force (Fmax) of each sample was determined isometrically. Once set this parameter, muscles were subjected to a series of isotonic releases from 0.9 to

0.1% of their Fmax during a train stimulation at 1A (pulse width: 0.2ms; pulse frequency: 150Hz; train duration: 1s). The contraction and relaxation velocities were then derived from these experiments.

Curve fitting

Force/velocity data were fitted to Hill's equation (Hill, 1938) using SigmaPlot's Dynamic Fit Wizard. The following form of Hill's equation was used:

$$(P + a)\, v = b\, (P_0 - P)$$

where P is the force during shortening/peak isometric force, v is the velocity of shortening (L_0/s), and a, b and P_0 are the adjustable constants. Vmax and 1/G (curvature of the relation) parameters were retrieved from the resulting fitting. In detail, Vmax corresponded to the intercept of the curve on the velocity axis, and 1/G that was calculated as

$$\frac{1}{G} = \frac{a}{P_{max}}$$

where P_{max} is the peak tetanic force. The fit was not constrained to pass through P=1.0.

3.5 Immunohistochemistry

Immunohistochemistry has been performed to localize DHPR, RyR and innexin within muscle tissue. 10-20µm sections were rinsed in 1×PBS, permeabilized in 1×PBS + 1% Triton X-100 (PBS-T) two times for 5 minutes at room temperature (RT) and incubated in blocking solution (PBS-T + 0.1% BSA + 10% goat serum) for 1h at RT. Primary antibodies in blocking solution were applied overnight at 4°C. Negative controls were incubated in

blocking solution without the antibody to avert unspecific bounds. After 3 PBS-T washes, sections were incubated in secondary antibodies (1:1000), Alexa Fluor™ 647 Phalloidin (F-actin; Life Technologies, Milan, Italy), and DAPI/Hoechst (nuclei; 1:1,000) 2h at RT. Tissues were rinsed several times and mounted in ProLong Gold antifade reagent (Life Technologies, Milan, Italy) for analysis. Primary antibodies were used as shown in table 1.

Table 1: Primary antibody dilutions and specifications

Antibody	Dilution	Manufacturer
Dihydropyridine Receptor alpha-1 Monoclonal Antibody (1A)	1:200	Thermo Fisher Scientific
RyR3	1:1000	Millipore
Innexin	1:500	Thermo Fisher Scientific

3.6 Image processing

Confocal imaging was performed using an inverted confocal laser microscope (Leica SP8) and three-dimensional reconstructions were generated using Leica Application Suit X (LAS-X) software.

Sirius red labeled sections were imaged using 561 nm excitation length, with the emission recorded at 592-634 nm, exploiting the staining autofluorescent properties.

3.7 Gene identification

3.7.1 RNA extraction and cDNA synthesis

Total RNA has been extracted from octopus brain and arms using RNeasy Microarray Tissue Mini Kit (Qiagen) and contaminating DNA has been degraded by treating each sample with RNase-Free DNase Set (Qiagen). For all RNA samples, purity of total RNA extracted has been estimated measuring both the absorbance ratios 260/280 nm and 260/230 nm by NanoDrop 1000 Spectrophotometer (Thermo Scientific). For each sample, 1µg of total RNA extracted have been retrotranscribed with ImProm-II(TM) Reverse Transcription System (Promega) following the manufacturer's instructions.

3.7.2 Gene sequencing and identification

mTOR and innexin unc-9 genes have been divided into small fragments up to 1.5kb and the correspondent primers were designed. 2µL of Octopus cDNA were used as a template for PCR.

Table 2: mTOR primers

Fragment	Primer Sequence	5'→3'	Amplicon length (bp)
1	ATGACATCCAAACATATAACTCC	Fw	783
	GTTACTGCATCGTAGAAGTTC	Rev	
2	GAACTTCTACGATGCAGTAAC	Fw	921
	ACCTTCAAAATCAAAACTGCCCAGAGT	Rev	
3	ACTCTGGGCAGTTTTGATTTTGAAGGT	Fw	858
	CTGCTCTGTTTTCATGAAATTAAGAAG	Rev	
4	CTTCTTAATTTCATGAAAACAGAGCAG	Fw	1278
	TAGCCACTCATTCCAGTCTTCTTTAGA	Rev	
5	TCTAAAGAAGACTGGAATGAGTGGCTA	Fw	999
	TCGCCGCTCTGGTATCAATTTGTACTG	Rev	
6	CAGTACAAATTGATACCAGAGCGGCGA	Fw	1470
	TTCCAAAGAAGTTAACTGAGG	Rev	

7	TTGAGGCCATACAGTGATGC	Fw	1005
	ACCTTCAAAATCAAAACTGCCCAGAGT	Rev	
8	GGGGAGAGCTTTGGAGACTT	Fw	1138
	CTGCTCTGTTTTCATGAAATTAAGAAG	Rev	
9	ACTCTGGGCAGTTTTGATTTTGAAGGT	Fw	972
	CAGCGTCAATCCAGATTCTTC	Rev	
10	TCAACCCCAGAACTAATACCTACC	Fw	1326
	TCGCCGCTCTGGTATCAATTTGTACTG	Rev	
11	TCTAAAGAAGACTGGAATGAGTGGCTA	Fw	1396
	TACGAAGTTCAGCGACAGCA	Rev	
12	TACAAGGCATGGCATGCGTGGG	Fw	921
	TTCCAAAGAAGTTAACTGAGG	Rev	
13	ATTGATTTTGGTGATTGTTTTGAAGT	Fw	441
	CTCTGGTTGAATCGGGTCAT	Rev	
14	TTTTAACACAACCGCCTTCC	Fw	398
	AAAGGCATCTCAGGAACATCA	Rev	

Table 3: Innexin unc-9 primers

Fragment	Primer Sequence	5'→3'	Amplicon length (bp)
1	GTGAGATCGACTTACTGTGCC	Fw	489
	ACTGGCAACACTCACAATG	Rev	
2	GTAGATCGCATTGTGAGTGTTGCC	Fw	609
	TGAGCCTATTCGATCCATGA	Rev	
3	GCTACAGTTTTGCTACATGGA	Fw	415
	CACGCACACTTGCATACAGA	Rev	
4	GCTACAGTTTTGCTACATGGA	Fw	299
	CTATACATCTTCACCTTCTG	Rev	
5	GATCGACTTACTGTGCCAAGC	Fw	493
	TGAGCATCACTGGCAACACT	Rev	
6	GGAAGATGGATGGACAGCAT	Fw	472
	TGTTACGGGTTCGGTTTTCT	Rev	

Fragments obtained from PCR have been purified and sequenced using automated Sanger method (Applied Biosystems 3130 DNA Analyzer). The identity of segments has been verified and analyzed by BLASTX and BLASTP programs. Consensus sequences were obtained from fragment overlap.

Octopus bimaculoides DHPR alpha1 and RyR genes were retrieved from the Metazome v 3.2 database from the University of California and conserved protein domains were assessed by NCBI Conserved Domain Database.

Protein sequences were aligned with the human, mouse or *C. elegans* sequences using ClustalW and protein similarities have been calculated using BLASTP at NCBI Genbank. Protein domain annotation and conservation level were assessed by NCBI Conserved Domain Database. For prediction of transmembrane helices and topology, TMHMM version 2.0 has been used. The presence of serine, threonine or tyrosine phosphorylation sites was predicted using NetPhos 3.1 server.

3.8 Biochemistry

3.8.1 Protein extraction

To obtain total cellular protein, 10-20mg of tissue have been homogenized (with Tissue Lyser) in 600µL of extraction buffer (NP40 1% - SDS 1% - Tris 50 mM pH 7,6 - NaCl 150 mM, protease inhibitor (Roche) and phosphatase inhibitor (Sigma)). After incubation for 5 min at 100°C, samples have been sonicated and a centrifugation step has been performed at 4°C for 15 min at 13000×rpm to remove cell debris. The supernatant was used for determination of protein amount by BCA test.

3.8.2 Western blot

80µg protein extracts were separated onto gradient pre-cast acrylamide gel (4-12%) at 70V and wet transferred onto nitrocellulose membranes (pore 0,2µm) overnight at 60mA at 4°C. Blotting was verified with Ponceau, the membrane was blocked in BSA 5% in TBS-Tween 20 for 1 hour and was probed with primary antibodies overnight at 4°C while shaking. Proteins of interest were detected with opportune secondary HRP-conjugated antibodies and visualized with the ChemiDoc MP System (BioRad).

Primary antibodies

Polyclonal **β-actin** (Sigma - diluted 1:50000) and **Phospho-mTOR** (Ser2448) (Cell signaling - diluted 1:5000) antibodies were chosen on the basis of the sequence similarity with respective rabbit and human epitopes used to develop the antibodies as shown in figure 23.

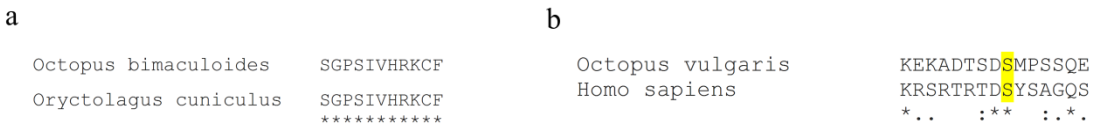

Figure 23: Antibody epitope alignment. a) *Octopus bimaculoides* and rabbit actin antibody epitope alignment. b) *Octopus vulgaris* and *Homo sapiens* mTOR protein alignment around Ser2448 (highlighted in yellow)

Based on the sequence identified, a custom octopus-specific innexin **unc-9** antibody was produced by Thermo Fisher (Thermo Fisher Scientific). The epitope was selected on the basis of its immunogenicity at the N-terminus intracellular site (aa 19-34: RLGKVKVRNDDDLIDR) and the correspondent peptide was synthetized. Two rabbits have been immunized and test-bleeds have been performed on serum 28, 56 and 72 days after injection. The most reactive serum has been selected and affinity purified (concentration: 0,90 mg/mL). The resulting antibody was employed at 1:500 dilution.

3.9 Electrophysiological measurements

3.9.1 Cell preparation

Small pieces of arm intrinsic musculature were dissected from either transversal or longitudinal muscles under a dissecting microscope. The tissue was incubated at 25-30°C for 4-6h in 0.2% collagenase (Sigma type I) dissolved in L15 culture medium (Sigma-Aldrich) adjusted to the concentration of salts in seawater. The enzymatic treatment was terminated by rinsing with fresh L15. The tissue was then triturated manually until an appreciable concentration of dissociated cells could be detected in the supernatant. Cells were plated on a plastic Petri dish and kept at 17°C up to 6 days.

3.9.2 Current clamp

All the electrophysiological measurements were performed on Axoclamp 2B (Axon Instruments) amplifier. Recordings were sampled at 20kHz, digitally stored and analyzed through a LabVIEW software. During the experiments, cells were continuously superfused with oxygenated ASW at room temperature. Glass pipettes were pulled on a pp-830 puller (Narishige) with a two-step procedure. The resistances of the pipettes were between 2–4 MΩ. The occurrence of contraction in the patched muscle cell was visually inspected.

Membrane potential of octopus arm myofibers was measured in a whole-cell current-clamp in single-electrode bridge mode. After the establishment of the whole-cell configuration, the cell membrane potential was brought to a holding potential of -80 -90 mV by injection of DC current. Muscle cell response was then induced by puffing of few nl of 1mM ACh in the vicinity of the cell center.

3.9.3 Solutions and drugs

The patch pipettes were filled with the following internal solution (in mM): 475 K-gluconate, 2 $MgCl_2$, 1 $CaCl_2$, 5 Na_2ATP, 0.5 Na_2GTP, and 50 HEPES, buffered to pH 7.2 with KOH. The free Ca^{2+} solutions contained (in mM) 460 NaCl, 10 KCl, 57 $MgCl_2$, 1 EGTA, 8 $CoCl_2$, 10 glucose, and 10 HEPES, pH 7.6 (adjusted with NaOH). For Ca^{2+} free experiment the patch pipettes were filled with the following internal solution (in mM): 475 K-gluconate, 3 $MgCl_2$, 5 Na_2ATP, 0.5 Na_2GTP, and 50 HEPES, buffered to pH 7.2 with KOH.

3.10 Electron microscopy

Bundles of longitudinal and transverse muscle fibers of approximately 3x2 mm^2 were dissected and briefly fixed in 4% PFA, 3% Glutaraldehyde in ASW for 4 hours. After several washes in ASW, samples were cut at 100µm with a vibratome. Sections were post-fixed in 1% OsO_4, 1.5% $K_4Fe(CN)_6$, 0.1M sodium cacodylate, *en bloc* stained with 10% of uranyl acetate replacement stain (EMS) for 30 min, dehydrated, infiltrated with propanol oxide and flat embedded in epoxy resin (Epon 812, TAAB). After baking for 48h, 1x1 mm pieces of tissue were excised from the block and mounted on a cured Epon block for sectioning using an EM UC6 ultramicrotome (Leica Microsystems). Ultrathin sections (60–70 nm thick) were collected on 200-mesh copper grids (EMS) and observed with a JEM-1011 electron microscope (Jeol, Tokyo, Japan) operating at 100 kV using an ORIUS SC1000 CCD camera (Gatan, Pleasanton, CA).

3.11 Statistical analysis

The software SigmaPlot 13.0 (Systat Software, Inc.) was used for statistical analysis. Normality of the dataset was first assessed with a normality test (Shapiro Wilk). Parametric t-tests and non-parametric Mann-Whitney Rank Sum Test were used accordingly to compare two data sets. ANOVA analysis was performed to compare multiple data sets. Where appropriate, the statistical significance was evaluated using a two-way ANOVA followed by a pairwise Holm-Sidak post hoc test. Dunn's Method was used when performing Multiple Comparisons versus Control Group. P values <0,05 were considered significant.

4. Results

4.1 Structural organization of the octopus arm

4.1.1 3D organization of transverse and longitudinal muscles along the arm

To obtain a comprehensive view on the organization of the transverse (inner) and longitudinal (outer) muscle layers composing the main arm muscular bulk, a fine morphological characterization of their arrangement at different arm length has been performed (for details see Materials and methods section figure 11 and 12).

The thickness of longitudinal and transverse muscle on the oral, aboral and lateral axes was measured on transverse sections from apical, central and basal portion of the arm (n=45, for 3 samples; figure 24a).

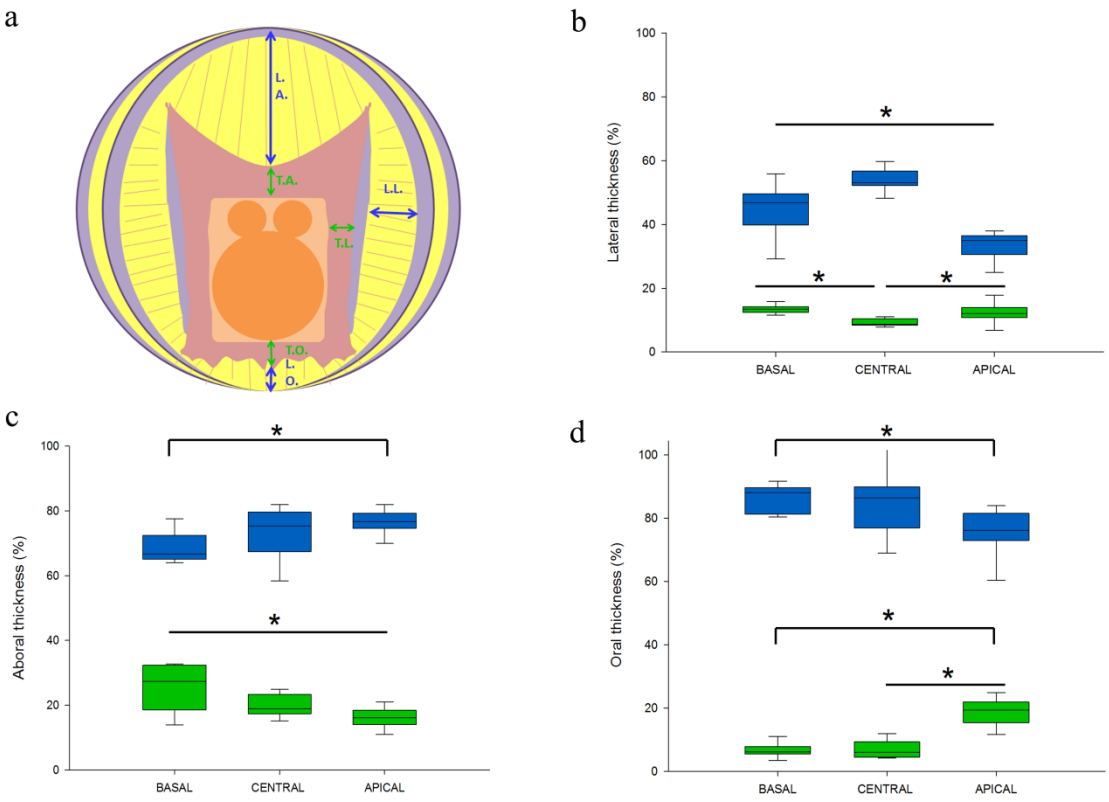

Figure 24: Organization of longitudinal and transverse muscles along the arm. a) Cartoon representing the measurement methodology. Box plot of longitudinal (blue) and transverse (green) thickness measured in basal central and apical arm portions at the lateral (b), aboral (c) and oral (d) regions (t-test, * P<0.05, n=45 for both experimental groups in each graph).

Lateral portions of the arm present a discontinue organization with longitudinal muscles (L.L.) occupying most of its space at basal and central location and decrementing at the arm tip and transverse muscles (T.L.) showing an opposite behavior (Figure 24b; t-test, P<0.05, n=45).

At the aboral side of the arm, a marked difference was found at the apical region where longitudinal muscles thickness (L.A.) tends to increase and that of transverse muscles (T.A.) to decrease (figure 24c; t-test, P<0.05, n=45). Conversely, oral transverse muscles thickness (T.O.) tends to increase and longitudinal muscles thickness (L.O.) to decrease (figure 24d; t-test, P<0.05, n=45).

Transverse muscles show a particular butterfly shape and insert within longitudinal muscles on the medial oblique muscle (M.O.M.). The length of transverse insertion (T.I.) on M.O.M. might have important biomechanical implications in motions such as torsion and therefore it was measured and expressed as a percentage of the X diagonal dimension shown in figure 25a.

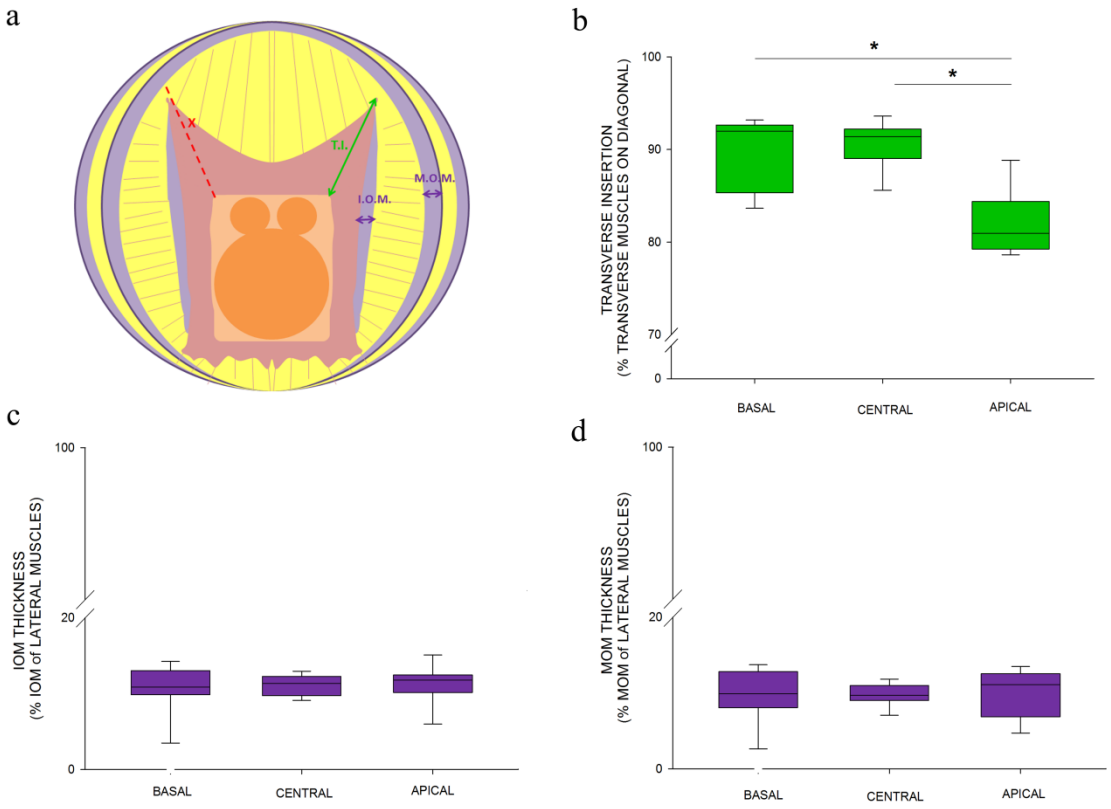

Figure 25: Transverse insertion (T.I.) and oblique muscle (O.M.) organization along the arm. a) Cartoon representing the measurement methodology. b) Box plot of transverse muscle insertion measured at basal central and apical arm segments (t-test., $P<0.05$, n=45). c-d) Box plot of medial (c; M.O.M.) and internal (d; I.O.M.) oblique muscle thickness measured at basal central and apical arm segments (ANOVA, * $P>0.05$, n=45).

Transverse insertion of transverse muscles (T.I.) on the median oblique muscle layer resulted to be significantly reduced at the arm tip (figure 25b; t-test, $P<0.05$, n=45).

As shown in figure 25c and d, both medial and internal oblique muscle thickness remains constant along the arm (ANOVA, P>0.05, n=45).

Overall, these results indicate that regional differences in arm muscle organization are manifested along the arm and are particularly evident at the arm tip. These findings might have an interesting correlation with the preferential use of arm portions as described by Mather (Mather, 1998).

4.1.2 Characterization of the elastic fiber architecture

Myofibers in the octopus arm are embedded in a dense connective matrix; this is known to play an important role in muscle biomechanics.

Here we focused on the architectural organization of coiled elastic fibers in transverse and longitudinal muscles as their amount and orientation can influence the energy stored and released during muscle deformations.

In order to characterize these aspects arm sections were stained with picrosirius red. Due to its autofluorescence, this commonly used histological technique allowed 3D visualization and reconstruction of collagen structure through confocal microscopy (Vogel et al., 2015) thus escaping from the antibody specificity problem (figure 26).

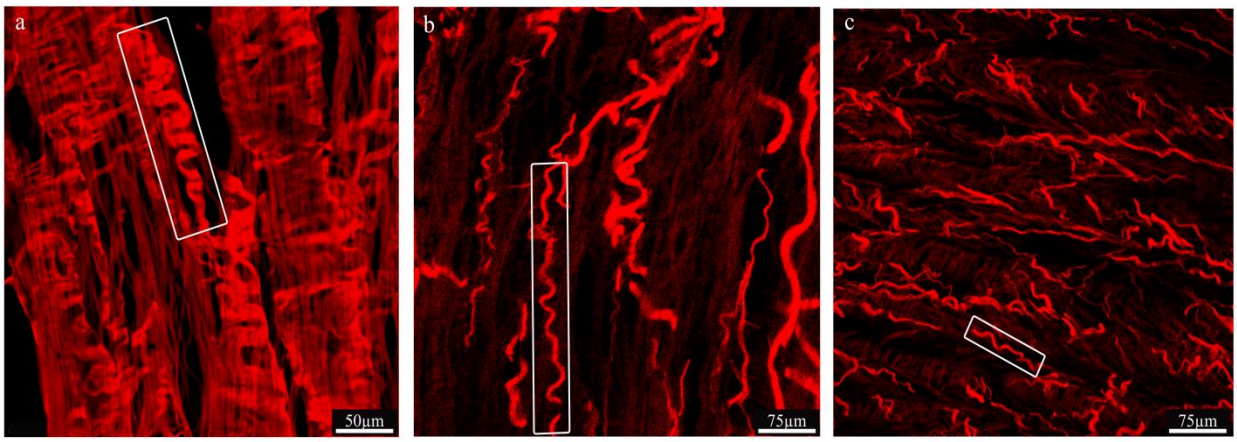

Figure 26: Confocal image of muscle stained with picrosirius red. Elastic supercoiled fibers (rectangle) appear intensely red over a less intense background. a) Longitudinal muscles. b) Transverse lateral muscles. c) Transverse aboral muscles.

Stained sections appeared pale red in most of the tissue compartments, but elastic fibers were clearly distinguishable for their characteristic coiled structure accompanied by an intense bright red coloration.

To evaluate the spatial distribution of elastic fibers, the angle between the elastic fiber axis and the main muscle longitudinal direction was measured (see Method 2.2) and defined as Chaos index (C.I.) (figure 27).

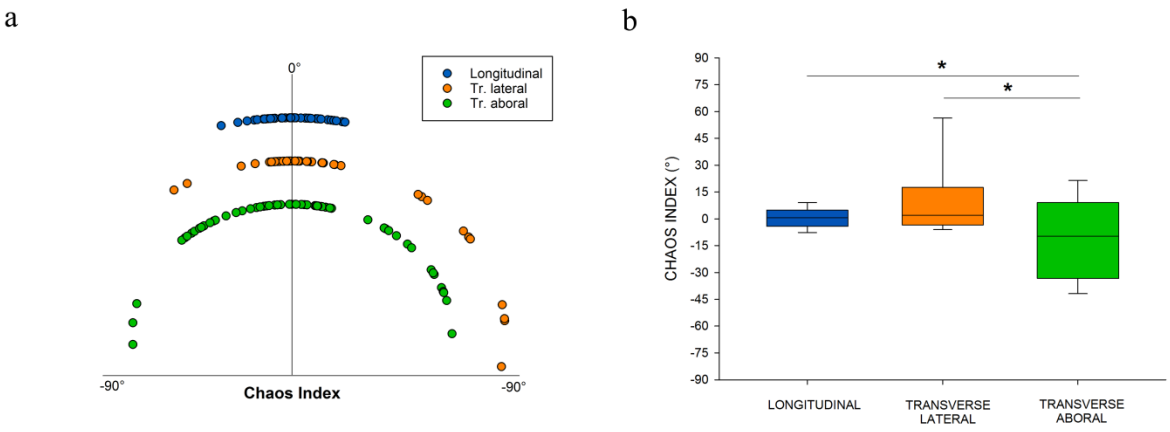

Figure 27: Chaos index analysis. a) Distribution of elastic fiber orientation respect to the main muscle force direction. b) Box plot of chaos index in longitudinal and transverse muscles. Longitudinal (blue), Transverse lateral (orange) and Transverse aboral (green) (Mann-Whitney, * $P<0.05$, n=60 for each experimental group).

Elastic fibers of longitudinal muscle were mainly oriented in the same direction of muscle cells (C.I. between -15° and +15°; n=60), while in transverse muscles were arranged in several orientations (-30°/+90° in T lateral (n=60); -90°/+90° in T aboral (n=60)). Due to their variable C.I., elastic fibers of the transverse aboral muscles were further divided in 2

subgroups on the bases of their rather parallel (Transverse Aboral par, C.I. within ± 20°) or non-parallel (Transverse Aboral no par, C.I. outside ± 20° range) orientation with respect to the orientation of muscle cells.

Quantification of the degree of folding of elastic fibers was then performed employing a dimensionless "waviness index" (figure 28a).

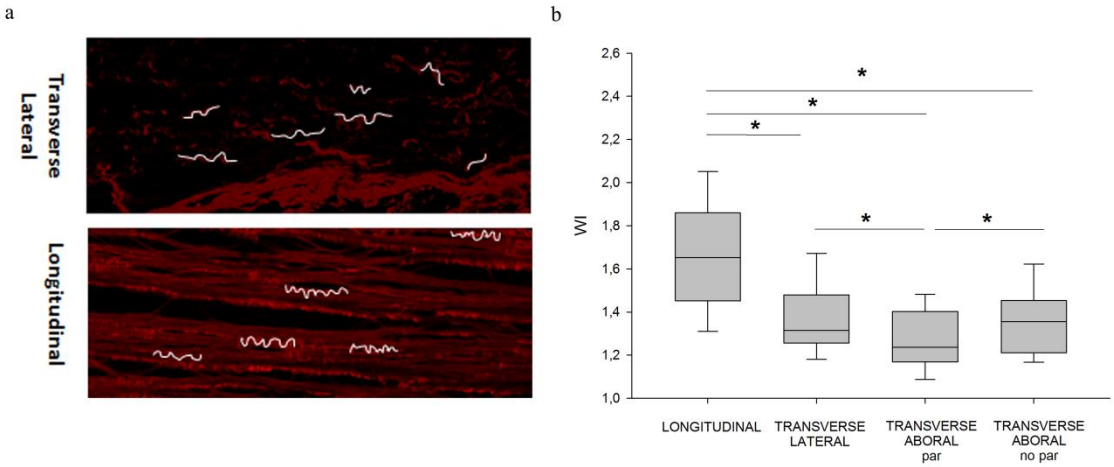

Figure 28: Waviness index analysis. a) Representative images of 3D reconstruction of transverse lateral and longitudinal muscle. b) Waviness index (WI) measures on different muscle types (t-test, * P<0.05, n=50 for each experimental group).

Elastic fibers of longitudinal muscles are significantly more folded than that of transverse muscles (figure 28b; t-test, P<0.05, n=50). These results indicate that there is a gradient in the waviness index between the inner and outer surface of the arm in the relaxed state. Such an arrangement may provide a means to passively adapt to whole arm strain during arm elongation. In order to test this hypothesis whole arm samples were subject to mechanical stretch from 10 to 30% of their resting length and immediately fixed while maintained in their stretched condition (figure 29a). Changes in W.I. in longitudinal muscles were then measured and found to be inversely correlated with the percentage of stretch (figure 29c). In the samples stretched to 30%, the fibers were almost unfolded, with a mean waviness index just above 1.0.

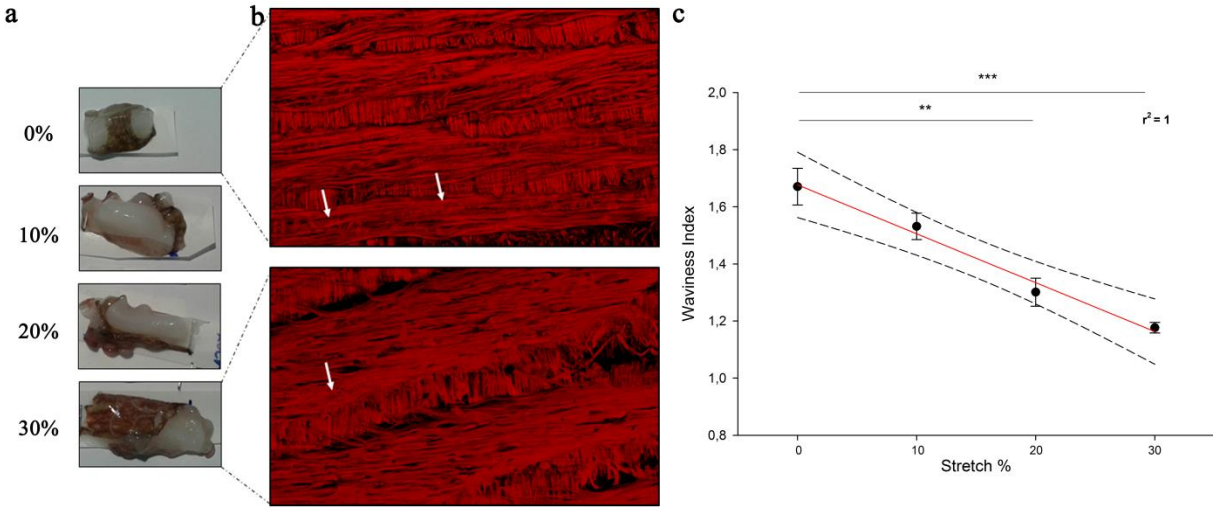

Figure 29: Arm mechanical stretch. a) Whole arm samples undergoing mechanical stretch from 0% to 30% L_0 b) Representative images of 3D reconstruction of longitudinal muscle stretched. Arrows indicate elastic fibers. c) Waviness index measured on longitudinal muscle stretched to 30% of their resting length. Dotted line: 95% Confidence Band (Multiple Comparisons versus Control Group (Dunn's Method). ** P<0.01, *** P<0.001; n=15 on 2 samples).

In summary, these muscles have an intrinsic different architectural arrangement of their elastic components and this is altered during arm deformation.

This opens the interesting possibility that transverse and longitudinal muscles differently contribute to arm motion exploiting their passive elastic properties. To investigate this point, biomechanical properties of both muscles were further assessed.

4.2 Muscle biomechanics

In order to investigate the mechanical characteristics of the octopus arm muscles, a Dual-Mode Lever Arm System has been used on in-vitro preparations of longitudinal and transverse muscles.

As mentioned in the material and methods section, based on the Hill's model, the forces generated in muscle samples have been dissected and described following the 3-element Hill muscle model (figure 17) as CE, PE and SE.

4.2.1 Passive properties

Passive properties of transverse and longitudinal muscles were investigated (i) under static conditions, with stepwise increments in stretch held for 5s, and (ii) under cyclic sinusoidal length changes.

(i) Repeated stretches from 1 to 30% of the initial muscle length were performed on L and T muscles and stress/strain profiles were used to quantify muscle stiffness (Figure 30).

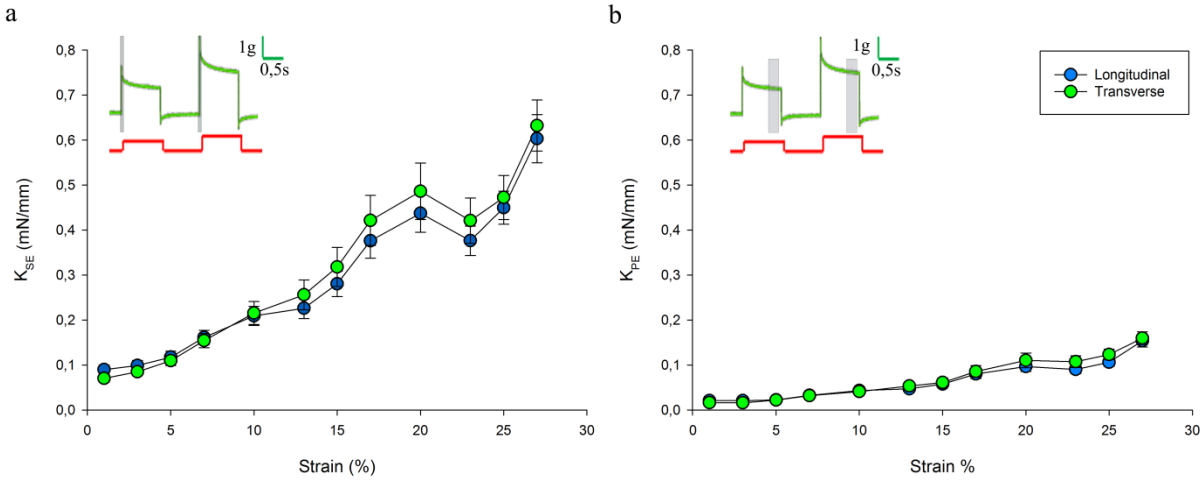

Figure 30: Muscle elastic stiffness. a) Longitudinal and transverse muscle elastic stiffness (K_{SE}). A sample trace of the step-stretch protocol with the peak-force analyzed (highlighted in grey). b)

Longitudinal and transverse muscle parallel elastic stiffness (K_{PE}). A sample trace of the stress-strain protocol with the plateau-force analyzed (highlighted in grey) (n=8 for both experimental groups).

Within the range of muscle stretch studied, both muscles show comparable values of stiffness with peak forces up to 5 folds higher that plateau forces (compare figure 30a and b). A nearly linear strain-stiffness relation was found in the first strain region (until ~15%) and a non-linear region at higher strain.

(ii) Cyclic deformations composed by a loading and an unloading phase were employed. Longitudinal and transverse muscles underwent 2.5Hz cyclic length change at an amplitude of ±30% of the initial length and hysteresis loops were obtained from the third and fourth cycles of strain. Within this strain rate, both muscle types produced stable responses at the third and fourth cycle (figure 31a). The hysteresis % was then calculated (see method section for details) and found to be significantly higher in longitudinal muscles (figure 31b).

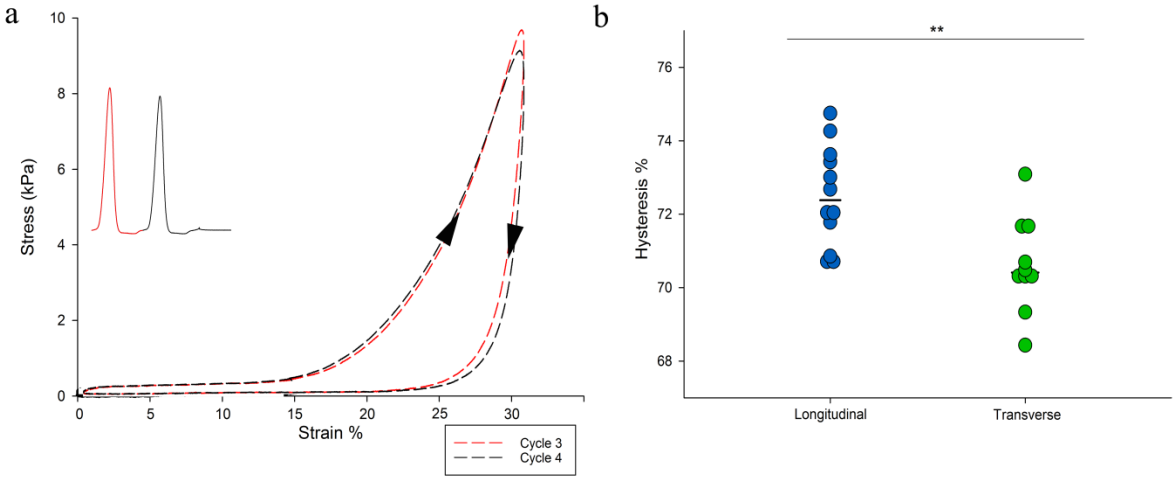

Figure 31: Hysteresis loop. a) Hysteresis loops and corresponding force trace obtained from the third and fourth cyclic sinusoidal length change. b) Hysteresis percentage for longitudinal and transverse muscle (t-test, ** P<0.01 n=10 for both experimental groups).

This indicates that longitudinal muscles manifest higher viscoelastic properties than transverse and this is particularly evident during the unloading phases of cyclic deformations.

This result well correlates with the presence in longitudinal muscles of a high amount of elastic fibers oriented toward the main muscle force direction that can release their energy in the unloading phase thus producing a higher hysteresis percentage.

This passive behavior can also influence the active muscle biomechanical properties. Indeed, upon muscle activation and contraction, elastic fibers are also subject to compression while during muscle relaxation they spring back to their resting state. Elastic fibers might then differently contribute to the phases of contraction and relaxation typical of muscles rhythmic activity.

To assess this point, active muscle biomechanical properties were next investigated.

4.2.2 Active properties

Active properties of transverse and longitudinal muscles were next investigated with isometric and isotonic protocols.

4.2.2.1 Muscle twitch properties

Longitudinal and transverse muscles response to twitch electrical stimulation (duration: 0.2ms, 1000mA) was measured evaluating the time to peak, the rate of contraction (dP), the ½ relaxation time and the rate of relaxation (−dP) (figure 32).

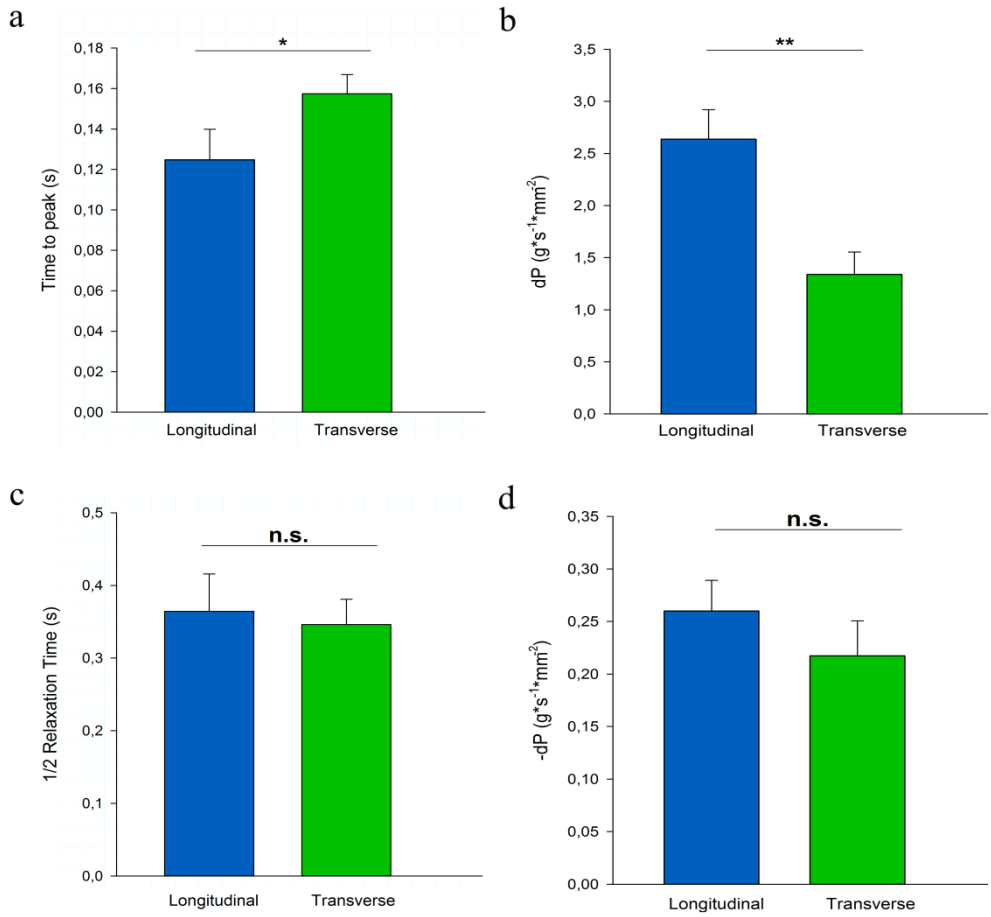

Figure 32: Parameters evaluated during a twitch in longitudinal and transverse muscles. a) Time to peak tension. b) Maximum rate of isometric contraction (dP). c) ½ Relaxation time. d) Maximum rate of isometric relaxation (-dP). Data are presented as mean ± standard error (t-test, *P<0.05, **P<0.01, n.s. not significant, n=6 for both experimental group for each graph).

Muscle twitch contraction time was longer in transverse (0.16±0.01s) than in longitudinal muscles (0.12±0.01s), as confirmed by the lower dP (T: 1.3±0.2g*s^{-1}*mm^{-2}; L: 2.6±0.3g*s^{-1}*mm^{-2}). During isometric relaxation, the ½ relaxation time and -dP were comparable between muscles (L: 0.36±0.05s – 0.26±0.03 g*s^{-1}*mm^{-2}; T: 0.35±0.03s - 0.22±0.03g*s^{-1}*mm^{-2}).

4.2.2.2 Length-tension relationship

The length-tension relationship was investigated measuring the twitch-force produced at increasing muscle stretch (figure 33a); from this protocol, it is possible to determine the muscle optimal length (L_{opt}). The length-tension relationship was built plotting the F/F_{opt} against L/L_{opt} for both muscles (figure 33b).

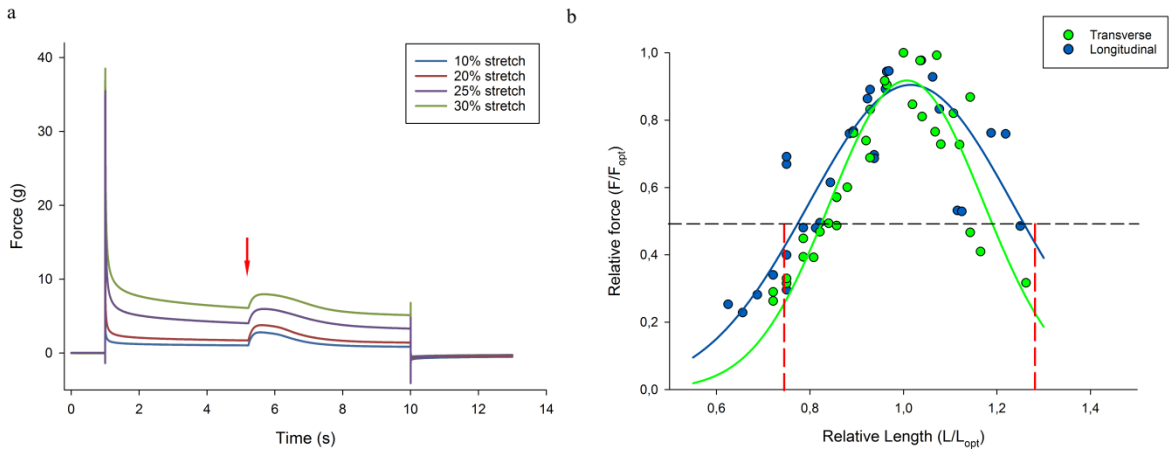

Figure 33: Length-tension relationship. a) Sample traces of muscle undergoing increasing step-stretch and twitch stimulated (red arrow). b) Active length-tension curves for L and T muscle. Force is expressed as F/F_{opt} where F_{opt} represent the maximum peak force of each preparation (F_{opt}), and length is expressed as L/L_{opt} where L_{opt} represents the length at which maximum peak force of each preparation was reached. Data were fitted using Gaussian 3 parameter equations. Red dashed lines highlight the length range that produced ≥0.5 F_{opt} (n=5 for both experimental groups).

The length–twitch tension relationships of the two preparation types did not show marked differences. The Gaussian 3 parameter equation fitting (solid lines in figure 33b) shows that both muscle types manifest the typical bell-shaped length-tension curve. Moreover, longitudinal and transverse muscles produced half of their F_{opt} over a wide range of lengths as highlighted by dashed lines in figure 33b. This behavior is typical of that of other hydrostatic muscles (Milligan, 1997; Kier and Curtin, 2002; Full and Meijer, 2004).

4.2.2.3 Muscle activation pattern

A force-frequency protocol was employed to investigate the activation properties of T and L muscles.

Muscles were stimulated at a frequency ranging from 1 to 100Hz and max force produced at each frequency was measured at L_0 (figure 34a). Sample forces were then normalized at their maximum and plotted against the stimulation frequency.

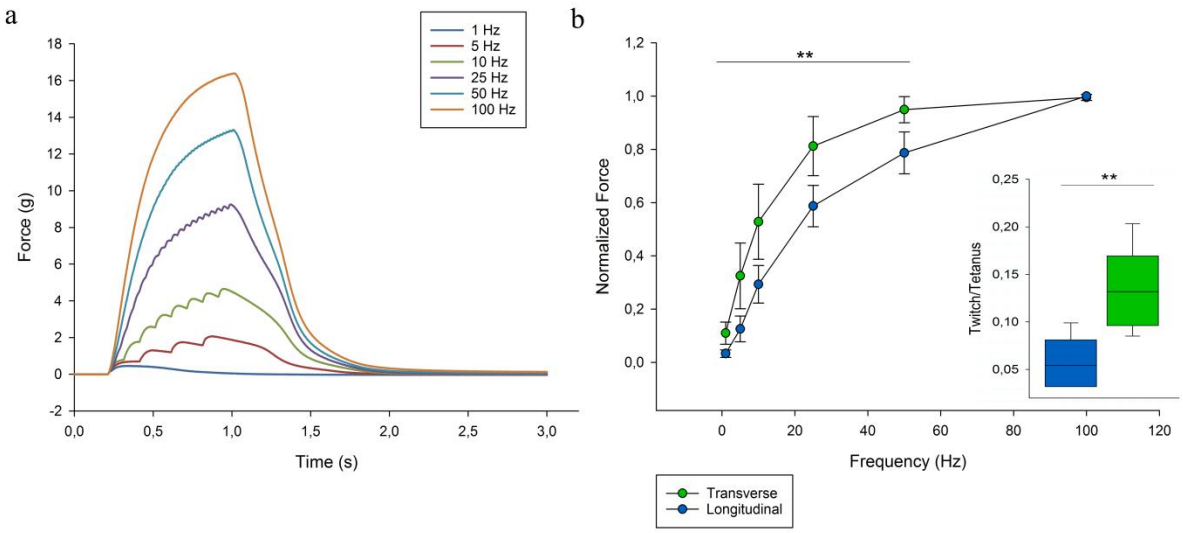

Figure 34: Force-frequency. (a) Sample traces of a single longitudinal preparation stimulated at frequencies ranging from 1 to 100 Hz. Summation and tetanization effects are visible at 5 and 50Hz respectively. (b) Force-Frequency relationship in longitudinal and transverse muscles. *Inset:* Twitch to Tetanus ratio. The tetanus force was measured at the 100Hz stimulation train in both T and L muscles (Mann-Whitney, ** $P<0.01$, $n=6$ for both experimental group).

The force-frequency relationship has a typical shape (figure 34b) with fusion frequency reached at 50Hz in both muscles. However, at any given submaximal stimulation frequency, transverse muscles produce a greater amount of force, thereafter the force-frequency curve is shifted to the left. This suggests that transverse muscles behave as slow-twitch fibers and

longitudinal as fast-twitch fibers. This difference is also highlighted by the twitch/tetanus ratio that is higher in transverse muscles (figure 34b, *inset*).

4.2.2.4 Mechanical work output

Mechanical work output was measured in order to study the effect of timing of the stimulation phase with respect to the muscle length. Muscles underwent cyclic sinusoidal length changes (±2% L_0; 0.5Hz) while sequentially stimulated at 0, 25, 50 and 75% of the cycle and force generated was measured (figure 35a,b). Work loops of longitudinal and transverse muscles were constructed plotting force vs length as shown in figure 35c.

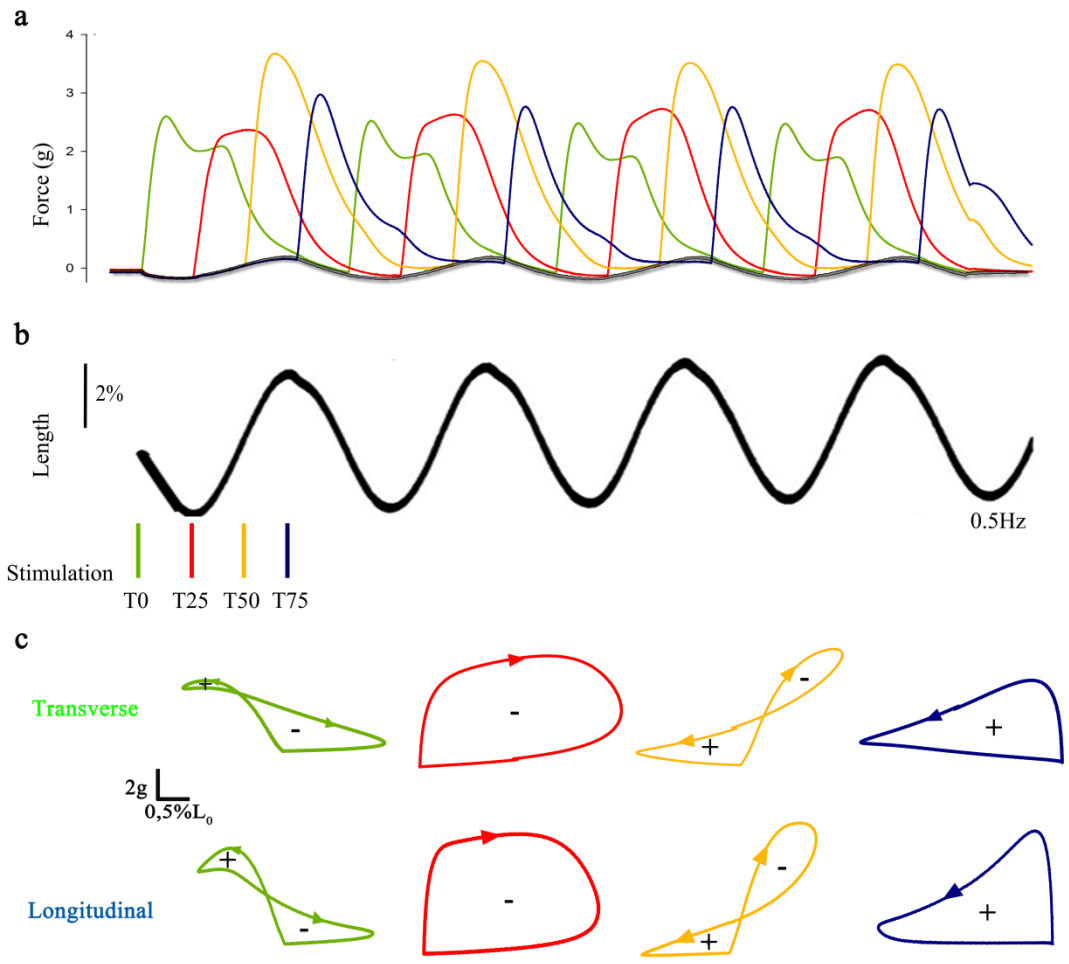

Figure 35: Work loop analysis. a) Exemplary force recordings of muscle fibers undergoing ±2% shortening-lengthening cycles (b) while stimulated at different time points. c) Corresponding work

loops for a longitudinal and a transverse muscle stimulated at different time point of the imposed cycle (green: T0; red: T25; orange: T50; blue: T75 – grey: no stimulation).

These images clearly show that the stimulation phase onset is determinant for the type of work produced.

As shown in figure 35, a gradual shift between positive to negative work and vice-versa was observed when the stimulation was applied during different phases of the sinusoidal cycle. Work loop shapes were similar in the two muscles at all the tested stimulation phase conditions. In particular, muscle activation during the first phases of shortening and lengthening, T0 and T50 respectively, led to a figure-eight work loop, with the sequential appearance of positive and negative work. When stimulation occurred at the maximum shortening phase, T25, transverse and longitudinal muscles generated negative work, while at the maximum lengthening phase, T75, they generated positive work.

Positive and negative works were then quantified from corresponding loops and net work was derived from them (figure 36).

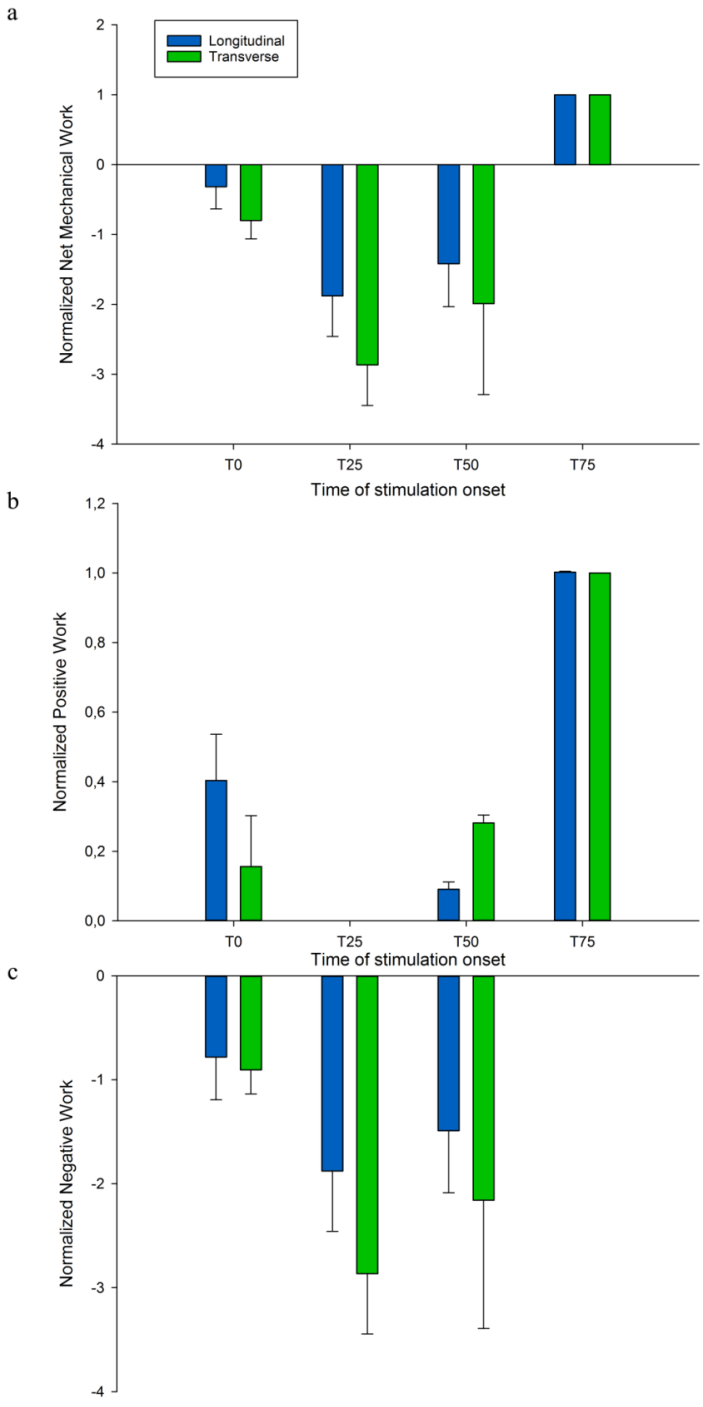

Figure 36: Longitudinal and transverse net, positive and negative work versus stimulation phase. Mean ± standard error of net (a), positive (b) and negative (c) mechanical work performed over a sinusoidal length change cycle for the longitudinal and transverse muscle (n=6).

Both muscles net mechanical work was approximatively zero at the onset of stimulation, T0, and negative at T25 and T50 with maximal energy absorption at T50. When muscle stimulation was delivered at the maximum lengthening phase, T75, muscles generated net positive work.

4.2.2.5 Force-velocity

The force-velocity relationship has been evaluated using isotonic shortening during 1-second 1A train (pulse width: 0.2ms; pulse frequency: 150Hz) imposing a Force from 10 to 90% of the sample Fmax (Fmax refers to the sample maximum isometric force; see material and methods section for details) (figure 37a,b).

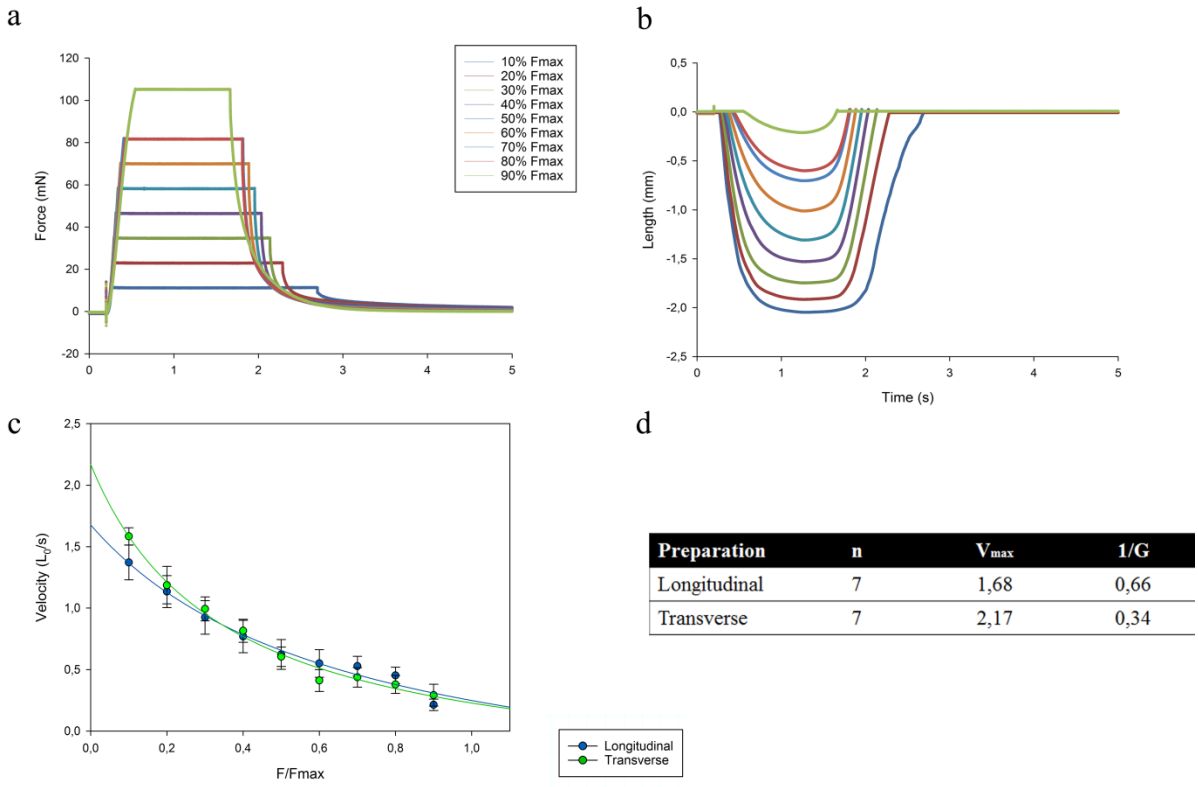

Preparation	n	V_{max}	1/G
Longitudinal	7	1,68	0,66
Transverse	7	2,17	0,34

Figure 37: Force-velocity relation. Typical traces of force (a) and length (b) excursion from a single experiment on a longitudinal preparation (imposed force from 10 to 90% Fmax). c) Force-velocity relation for longitudinal and transverse muscles. Force was reported as F/Fmax. The lines were fitted

to the data using Hill's hyperbolic function (see method) d) Force/velocity parameters of fiber bundle preparations. The values are from fits to Hill's equation (see method) (n=7).

The table in figure 37d shows the values of the fitted parameters for Hill's equation for longitudinal and transverse muscle. The maximum velocity of contraction of the longitudinal muscle was estimated to be 1.68 L_0/s, while the one of transverse muscle was 2.17 L_0/s.

The velocity of relaxation was also calculated in isotonic condition (figure 38).

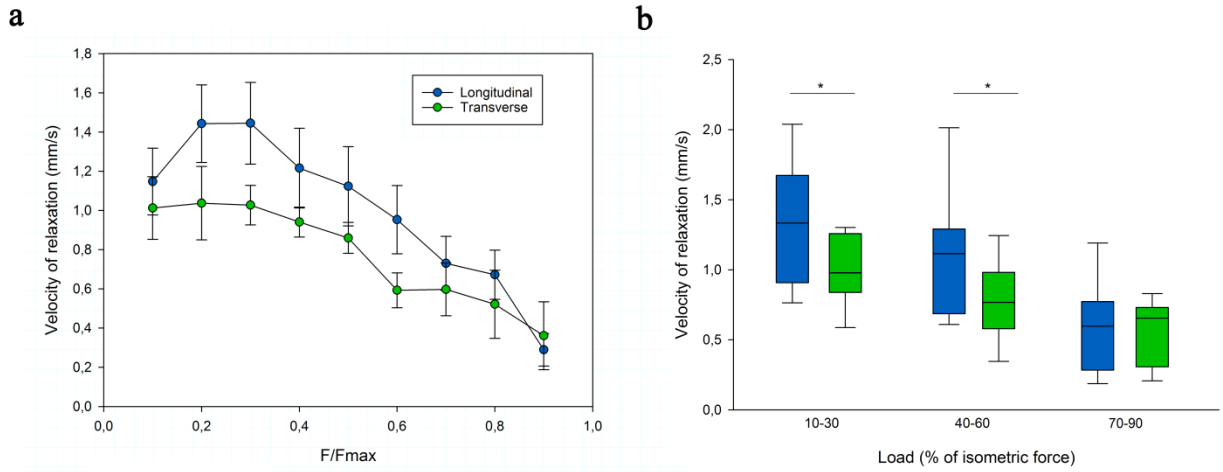

Figure 38: Relaxation velocity. a) Force-Velocity of relaxation curve. b) Box plot shows the velocity of relaxation at different load intervals. (t-test, * P<0.05, n=6).

The velocity of relaxation at low (10-30%) and medium (40-60%) load range was significantly higher in longitudinal than in transverse muscles (t-test, P<0.05), while at high load range (70-90%) no difference was detected (t-test, P>0.05).

4.3 Fatigue processes: the role of mTOR

mTOR is a highly conserved protein involved in sensing of cellular nutrition and energy status and its molecular pathway is related to the muscle resting/stress/exercise state. A particular class of exercise, defined as Resistance Exercise (RE), is known to activate mTORC1 and results in an increase in myofibrillar protein synthesis and muscle mass.

In order to evaluate the RE-induced activation of mTOR as a marker of response to exercise and fatigue, *Octopus vulgaris* mTOR has been first sequenced (sequence submitted to Genbank (Accession number: KY774846)). A domain annotation analysis was made, and results are shown in figure 39.

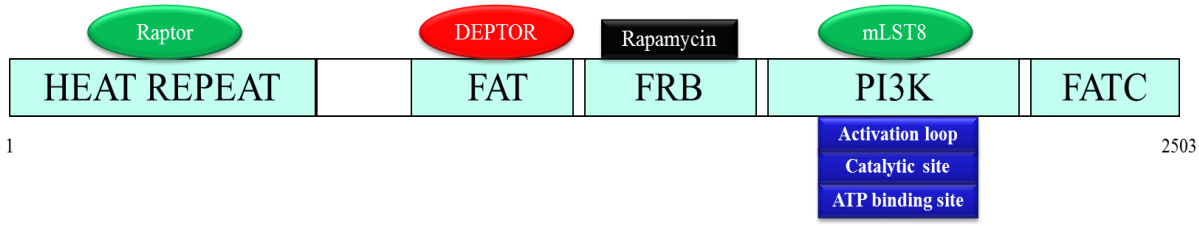

Figure 39: *Octopus vulgaris* mTOR conserved domains and its interacting protein.

All the vertebrate mTOR domains were found to be conserved, in details:

- HEAT domain at the N-terminus, which interacts with RAPTOR, a scaffold protein that recruits other mTORC1 substrates;
- FAT domain that binds DEPTOR, an inhibitor of mTOR;
- FRB which is the target for rapamycin, a macrolide that inhibits mTOR signaling pathway;
- PI3Kinase domain that has a catalytic function and has the phosphorylation sites that activate the protein;

- FATC domain, at the COOH-terminus.

Protein BLAST revealed that S2448 and S2481, whose phosphorylation is involved in mTORC1 and mTORC2 activation respectively, are conserved (figure 40).

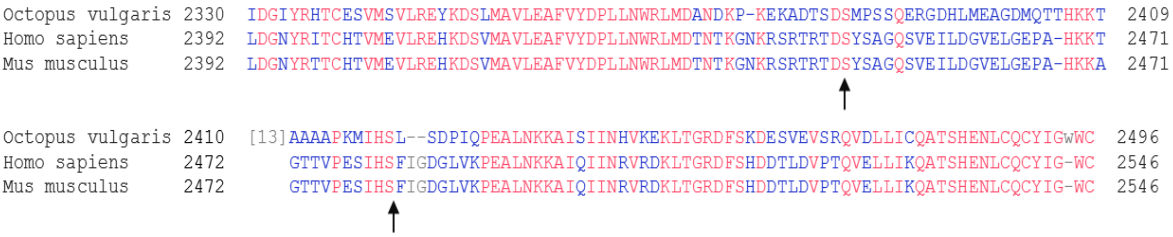

Figure 40: mTOR protein alignment in the region of the conserved phosphorylation sites.

4.3.1 Induction of muscle fatigue

A resistance protocol (RE) was specifically designed to induce muscle fatigue and consisted of three tetanic stimulation (pulse width: 0.2ms; pulse frequency: 100Hz; train duration: 3s; stimulation amplitude: 1A) repeated 7 times with an interval of 120 seconds. Typical experimental traces are shown in figure 41a where a clear reduction of the initial muscle force is observed at the third repetition of the protocol.

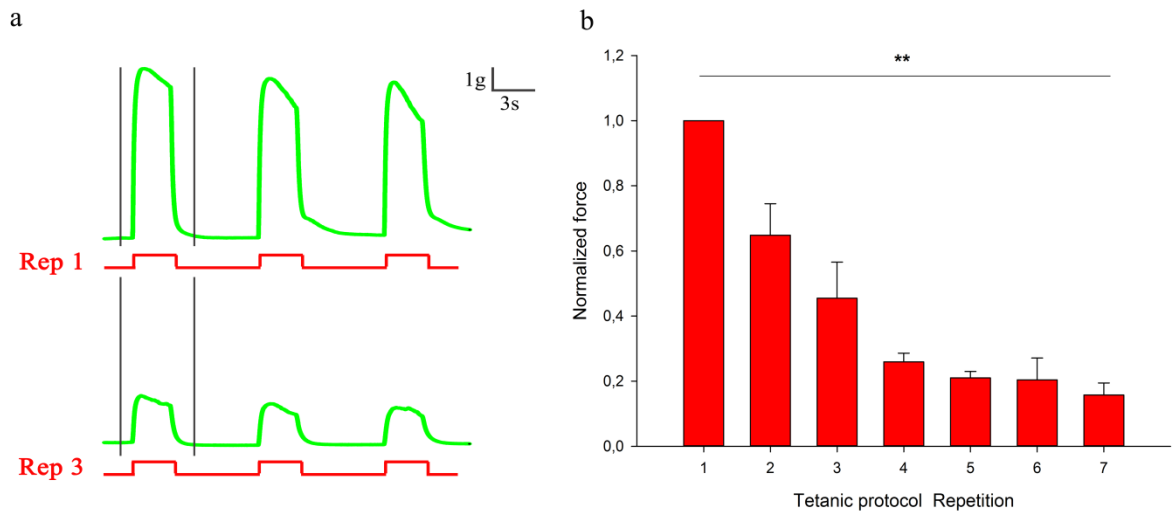

Figure 41: Muscle fatigue response. a) Tetanic protocol (red; pulse width: 0.2ms;

pulse frequency: 100Hz) designed to induce muscle fatigue response (green). Two repetitions of the same protocol have been reported (Rep1 and Rep 3). Maximum peak force has been analyzed for the first tetanus of each repetition (highlighted with gray bars). b) Maximum muscle force registered during RE protocol. Maximum force was analyzed for the first tetanic stimulation of each repetition (Mann-Whitney Rank Sum Test, ** P<0.01 versus control; n=6).

Measurements of the first tetanic stimulation response per each protocol show that the decrease in force reaches over 80% of the initial values (Figure 41b). This decrease is a typical indication of muscle fatigue induction. After the fourth repetition, tension generated reached a plateau.

Muscle samples were collected at different time points after the fatigue protocol (0, 30, 60 and 120 min) and prepared to biochemically characterize the mTOR activation profile (figure 42).

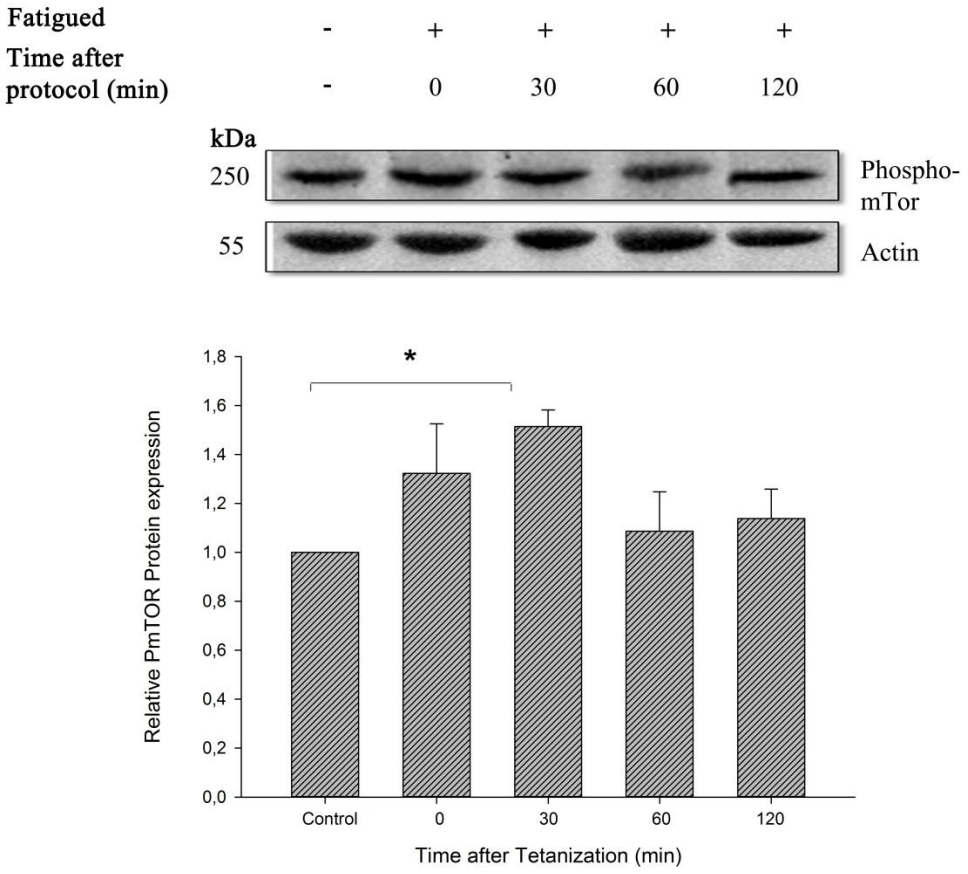

Figure 42: Effect of muscle fatigue induction on the mTOR pathway. Western blot and relative quantification of Phosphorylated mTOR expression in muscles undergoing RE protocol and collected at different time points after the end of the protocol (0, 30, 60 and 120 minutes). Samples were expressed relative to the control and normalized to β-actin (Mann-Whitney Rank Sum Test, * $P<0.05$ versus control; n=4 for each experimental group).

Quantification analysis revealed a gradual increase of mTOR phosphorylation at Ser^{2448} reaching a pick 30 minutes after tetanization (figure 42; $P<0.05$ versus control). mTOR phosphorylation returned to pre-fatigued value within 60 minutes from the end of the RE.

4.4 Mechanisms of excitation-contraction coupling

4.4.1 Role of internal calcium stores

We next wanted to elucidate the role of calcium internal stores in muscle contraction dynamics. To investigate this issue, we first stimulated by current injection and recorded the response of isolated muscle cells suspended in a Ca^{2+} free ASW. As depicted in figure 43a, stimulating single muscle cells in the presence of Ca^{2+} free ASW eliminated both action potentials and muscle contractions (data not shown). This indicates that external Ca^{2+} is vital for the generation of muscle action potentials and likely for the initiation of contraction. Moreover, it suggests that release of Ca^{2+} from internal stores, if exist, is Ca^{2+} dependent rather than voltage-dependent. To test this possibility, we applied 10mM caffeine in the same Ca^{2+} free solution to possibly induce Ca^{2+} efflux from internal stores (likely the terminal cisternae) and indeed following the application of caffeine the cells responded with a slow transient membrane depolarization and contraction (figure 43b). As Ca^{2+} was not entering the cell from the external solution and caffeine induces depletion of internal Ca^{2+} stores in muscles cells, internal Ca^{2+} stores must be present in these muscle cells. The releasing process might be mediated by a voltage-independent mechanism presumably "Ca^{2+} induced Ca^{2+} release".

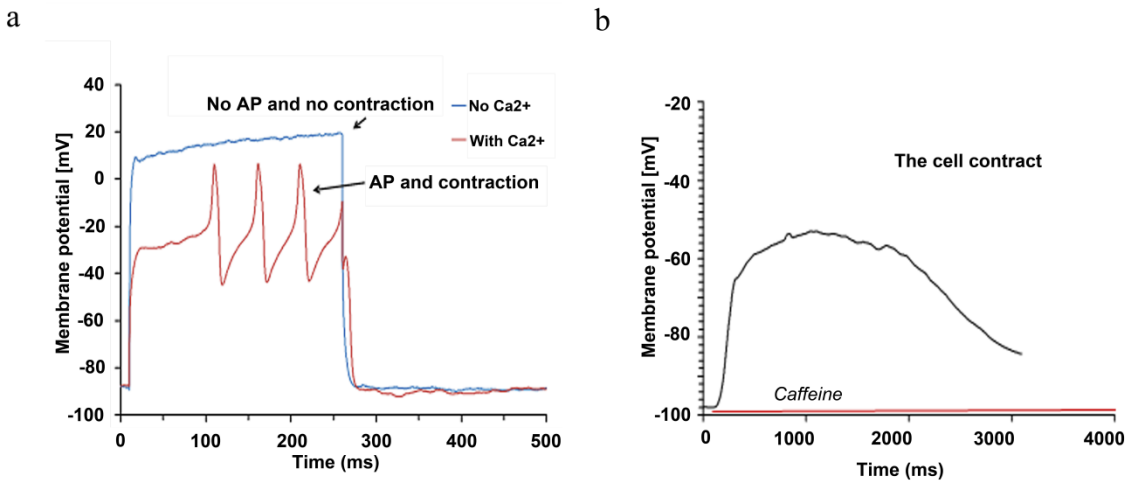

Figure 43: The role of Ca^{2+} in arm muscle E-C coupling. a) Muscle cells that were suspended in ASW respond to current injection stimulation with action potential and contraction (red). Nor action potential neither contraction were observed in response to current injection stimulation in the same muscle cells after replacement of the external buffer to Ca^{2+} free ASW (blue). (n=16). b) Application of 10mM caffeine in Ca^{2+} free external buffer evoked membrane depolarization and contraction of muscle cells (n=15).

4.4.2 Octopus excitation-contraction coupling machinery

Through a bioinformatic analysis, the predicted DHPR alpha1 subunit and RyR genes were identified in the sequenced genome of the closely related *Octopus bimaculoides* species (figure 44).

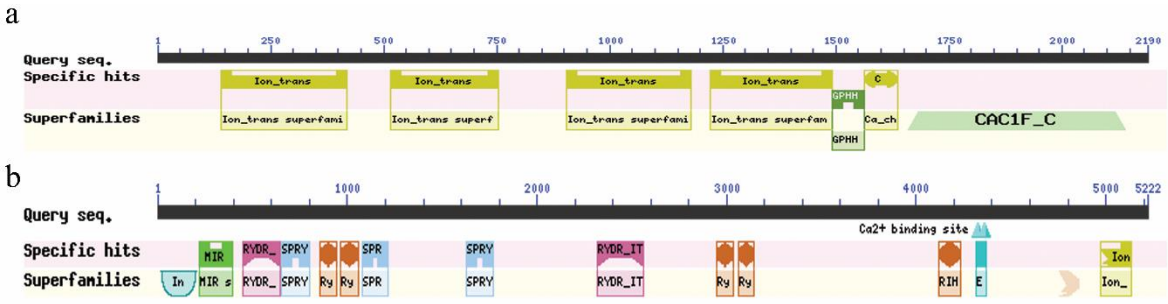

Figure 44: Octopus bimaculoides DHPR alpha1 (a) subunit and RyR (b) sequence and conserved domains.

Octopus DHPR alpha1 subunit (2190 aminoacidic residues) shares a 62% of amino acids identity and 75% of similarity with the human alpha1_C, which is one of the subunits forming the cardiac L-type voltage-dependent calcium channel. The main domains involved in the channel functions are conserved, including the four homologous repeats of transmembrane helices (Ion_trans) that constitute the pore, the voltage-gated calcium channel IQ domain (Ca_chan_IQ) that regulates cellular calcium flux and GPHH, a motif closely associated with IQ and found in voltage-dependent L-type calcium channel proteins in eukaryotes (figure 44a).

Octopus RyR shares 50% of amino acids identity with the human RyR type3, with the main domains involved in the channel functions conserved (figure 44b). Among these, three SPRY domains, that are important for protein-protein interaction and may represent docking sites for DHPR, and EF hands and Ca^{2+} binding sites at the C terminus domain.

The presence of DHPR and RyR on octopus muscle fibers was detected at the confocal microscope using human monoclonal and polyclonal antibodies, respectively, and both receptors were found to be located along the sarcolemma (figure 45).

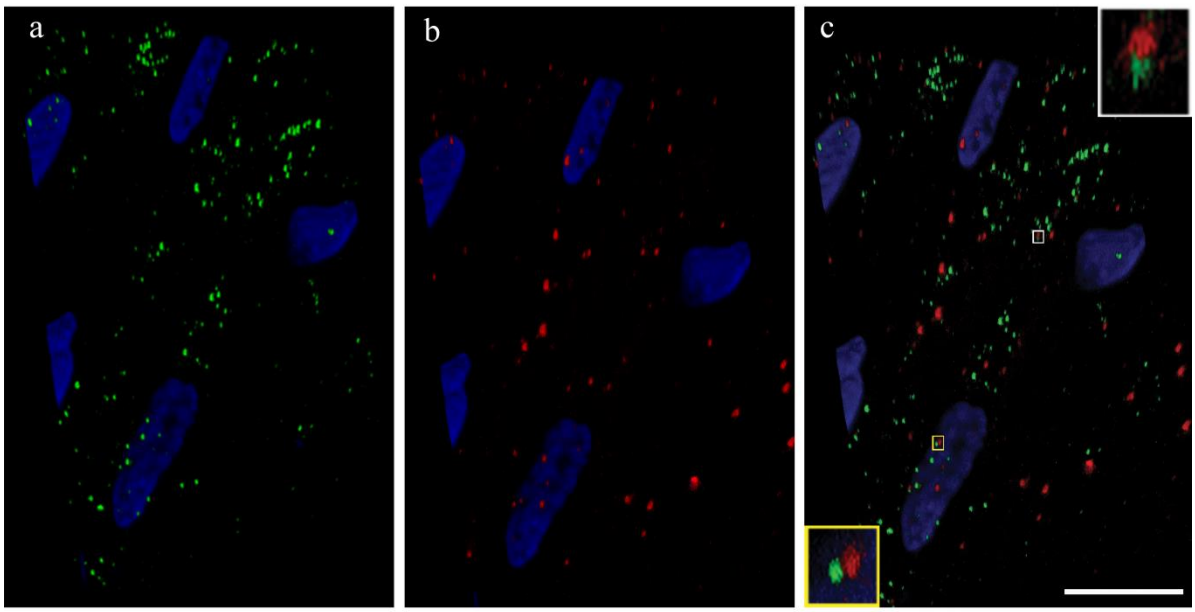

Figure 45: Immunofluorescence localization of (a) DHPR alpha1 (green) and (b) RyR (red) on sections of arm longitudinal muscle fibers (Blue: DAPI). c) Merged image of a and b and insets highlighting the colocalization of DHPR and RyR. Scale bar is 10µm.

A detailed co-distribution analysis and 3D reconstruction of the double-labeled samples revealed also that the two proteins are located in close vicinity at specific locations across the sarcolemma. It is reasonable to speculate that these locations might correspond to the points where sub-sarcolemmal cisternae are present and thus represent the functional link between sarcolemmal (junctional) events and calcium release from intracellular stores.

4.5 Coordination of muscle ensemble

4.5.1 Identification of muscular gap junction

In order to study the possibility that arm muscles are coordinated through gap junction, a bioinformatics analysis was performed to investigate the presence of invertebrate muscle-enriched gap junction genes.

The octopus unc-9 like innexin was identified and sequenced finding a 64% of positivity and a comparable topology with *C. elegans* unc-9 (figure 46).

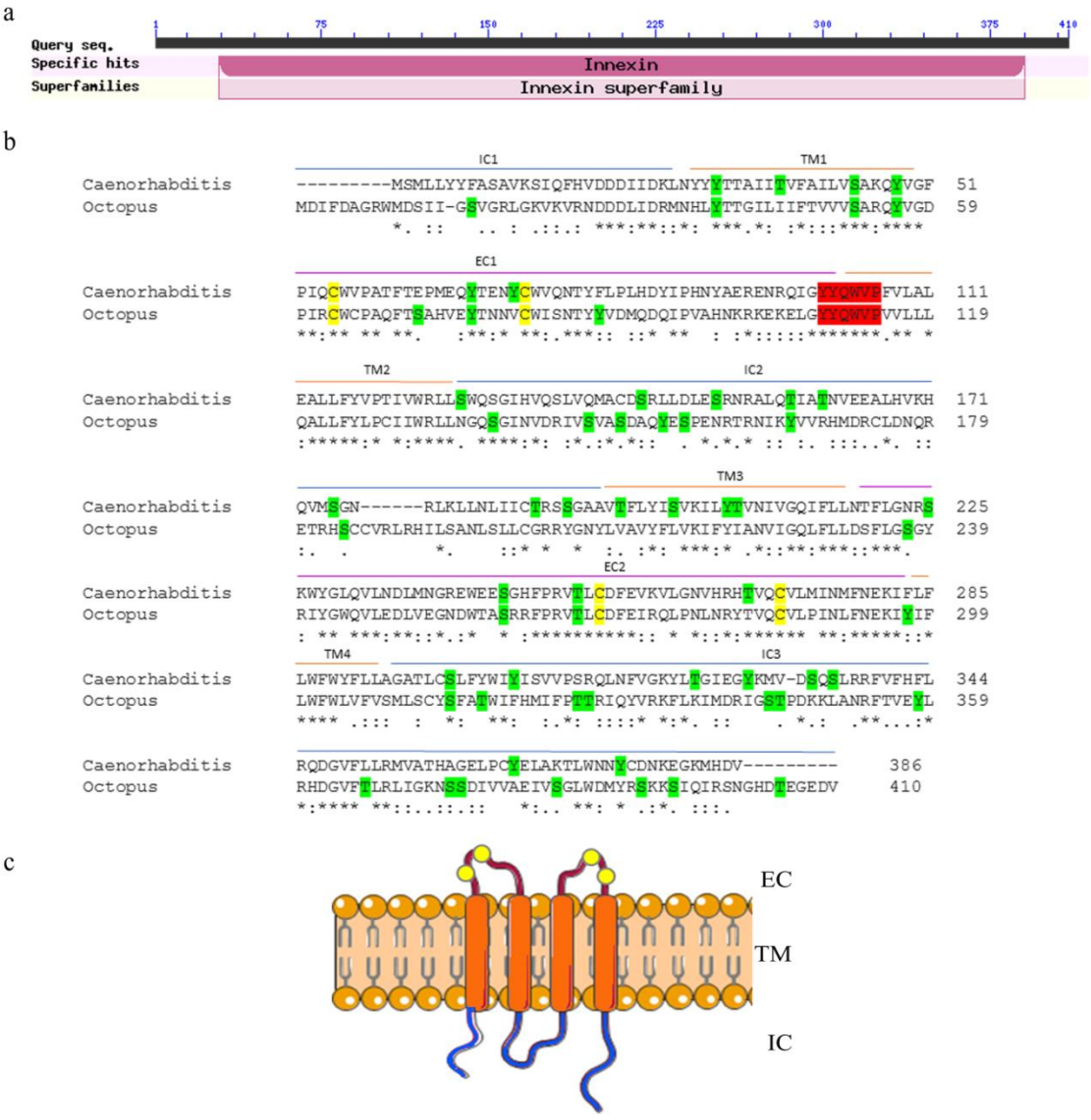

Figure 46: *Octopus vulgaris* unc-9. a) *O. vulgaris* unc-9 conserved domains. b) *O. vulgaris* and *C. elegans* unc-9 protein sequence alignment. Predicted phosphorylation sites are indicated in green;

conserved cysteine residues in the extracellular loops are highlighted in yellow; the conserved YYQWV motif is shown in red. c) Octopus innexin unc-9 topology. Intracellular (IC), transmembrane (TM) and extracellular (EC) domains are indicated by blue, orange and violet bars, respectively. Conserved cysteine residues are represented in yellow.

Alignment also revealed the presence of the conserved four transmembrane domains, the cysteine residues in the extracellular loops and the pentapeptide motif YYQWV located near the end of the first extracellular loop (in red in figure 46b) that is an innexin signature (Yen et al., 2007).

An antigenic epitope at the N-terminus of the protein (aa 19-34), located at the intracellular side was then selected for the production of a custom and purified rabbit antibody (*Thermo Fisher Scientific*) (figure 47a).

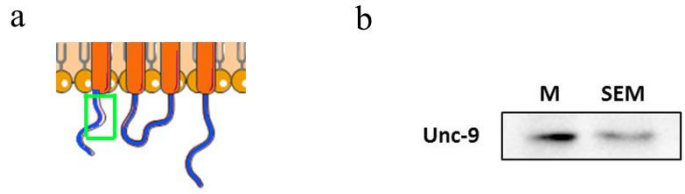

Figure 47: unc-9 antibody validation. a) The selected region for innexin unc-9 antibody production is highlighted in green. b) unc-9 antibody validation by western blot. (M: muscle; SEM: supraesophageal mass)

Innexin unc-9 antibody specificity was evaluated with western blot analysis and was found to have a strong affinity for octopus arm muscles (figure 47b).

Innexin unc-9 expression was revealed on octopus arm sections through immunohistochemistry that presented a punctate labeling with regular arrangement along adjacent sarcolemma (figure 48).

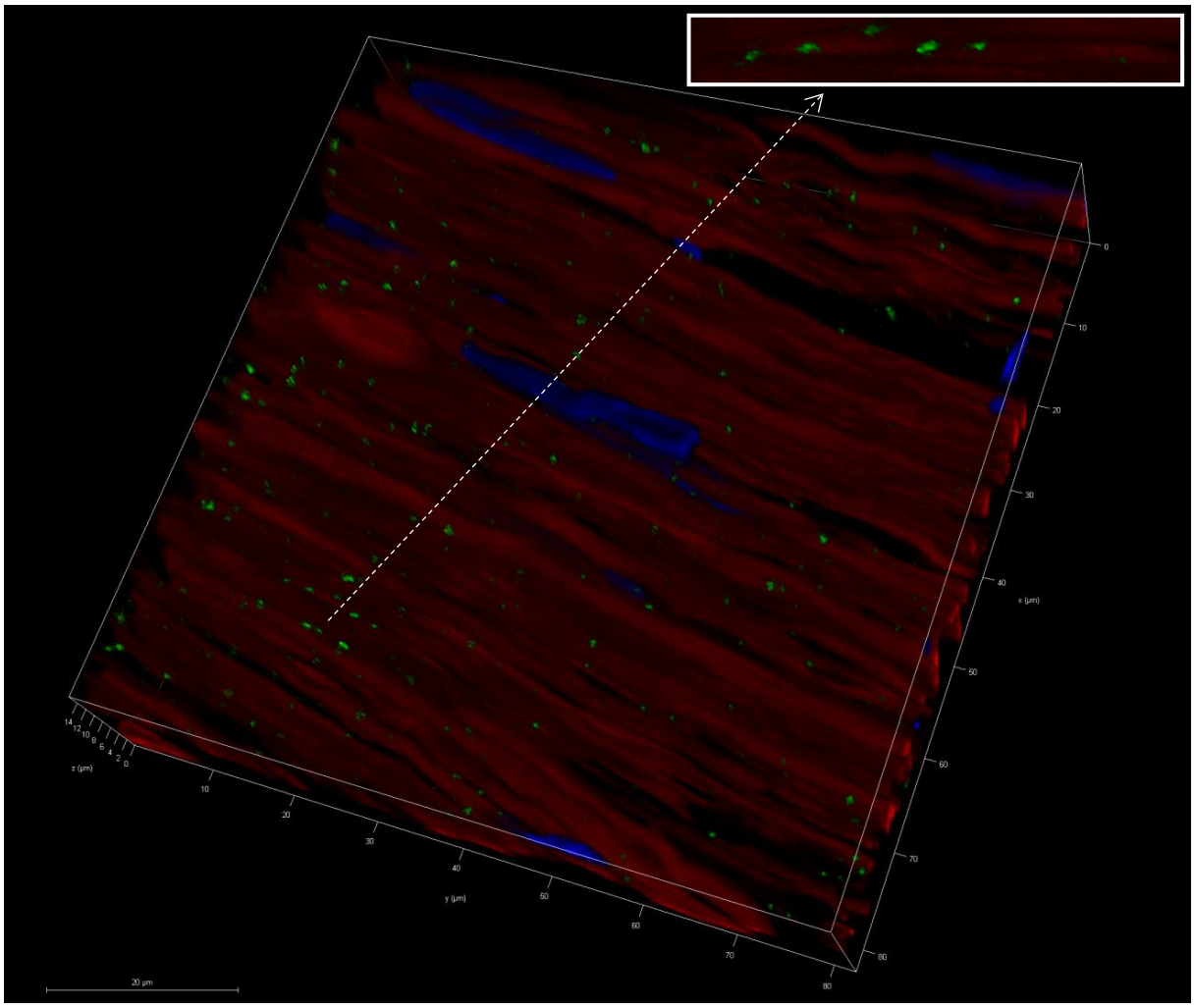

Figure 48: unc-9 expression on an arm muscle section. Confocal 3D reconstruction of innexin unc-9 localization along muscle fibers: (Blue: Hoechst; Green: innexin; Red: Phalloidin). *Inset*: magnification of a single fiber.

Gap junctions were also observed in transmission electron microscopy on ultrathin longitudinal and transverse muscle sections. Here, gap junctions were clearly identifiable as areas where the sarcolemma of two adjacent myocytes juxtapose at the level of a small electron-dense gap (figure 49).

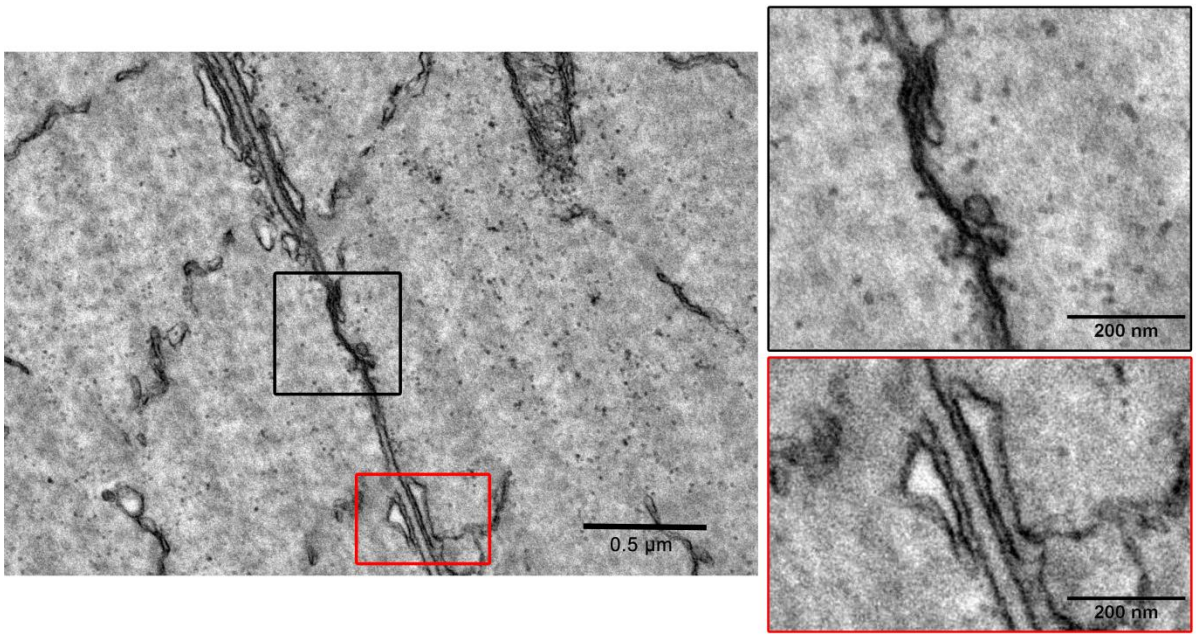

Figure 49: Gap junctions. Electron micrograph of thin sections of octopus transverse muscles showing the typical electron-dense gap junction structure (black squared) and the wider gap (red squared) at the two adjacent sarcolemma.

4.5.2 Functional relevance of muscular gap junctions

The existence of a functional coupling in arm muscle fibers was investigated using octanol (2.5mM in ASW), a known gap junction blocker, on in-vitro preparations. Twitch response (0.2ms, 1000mA) was tested in the presence and absence of octanol at 3min intervals. Control measurements were taken in the same condition used for octanol treatment to monitor the stability of muscle response over time (see material and methods section for details). As it can be seen in figure 50, a non-significant increase in twitch force, possibly due to a slight increase in the bath temperature, is manifested over time in the control condition (two-way ANOVA, $P>0.05$).

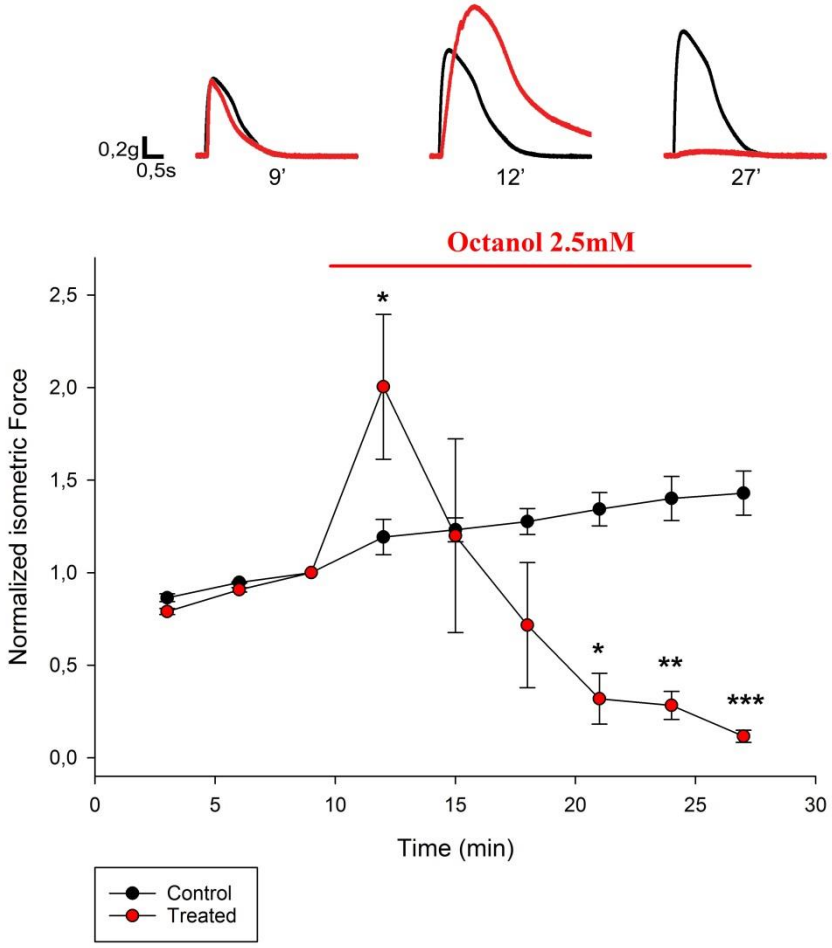

Figure 50: Effect of 2.5mM octanol on the maximum isometric force. Twitch recordings before (9') and after (12' and 27') the application of octanol shown (Two-way ANOVA: time ($P>0.05$), treatment ($P<0.01$) time x treatment ($P<0.01$). * $P<0.05$; ** $P<0.01$; *** $P<0.001$, Holm-Sidak post hoc test. n=6 for both experimental groups).

After 3 minutes of octanol exposure a transient significant increase of twitch force was recorded (two-way ANOVA, $P<0.05$), followed by a complete drop of muscle tension (two-way ANOVA, t21': $P<0.05$; t24': $P<0.01$; t27': $P<0.001$). No recovery of treated samples was recorded after up to 30 minutes continuous wash with normal ASW. Given the cooperative role of muscle elements during force production, this reduction in force can be explained by a

massive uncoupling of gap junctions in neighboring muscles although additional effects of octanol on other cellular pathways cannot be entirely excluded.

Taken together these results suggest that gap junctions are indeed present on the arm muscles and important for muscle cell ensembles coordination.

5. Discussion

The *Octopus vulgaris* arm is a highly flexible structure with virtually unlimited degrees of freedom (Kier and Smith, 1985). Indeed, the lack of any skeletal support enables the animal to move its arms in any direction and to perform complex tasks. In this study, we investigated the bases of this flexibility at various level of the arm organization.

Here we show that a morpho-functional specialization is indeed present along the arm. In particular, the inner and outer portions of the arm bulk, respectively the transverse and the longitudinal muscle layers, are differently represented at the arm apical region. This is in line with a regional specification of the arm nervous system as previously reported (Fossati et al., 2011). This feature might underlay the preferential use of specific arm portions during certain behaviors. Interestingly, several examples of this kind have been reported, among them, a preferential use of the distal arm section has been found during octopus exploratory actions (Mather, 1998). In this typical behavior, only the arm tips move along the surface of the substrate with the suckers performing a chemotactile search. Another example of the same kind can be seen during arm crawling, that involves the shortening of the proximal arm segment followed by the anchoring to the substrate mediated by suckers and then the elongation of the proximal segment (Levy et al., 2015).

It is interesting to notice that these complex motions can be achieved despite the absence of rigid elements typical of any hydrostatic limb. Here, quasi-articulated structures and joints can be formed at any point along the arms through the activation of antagonistic muscles and their intrinsic interaction with a dense connective matrix. Connective tissue is a fundamental element of hydrostatic muscles and can act in various manner depending on its structural organization and position along the body (Kier and Stella, 2007). Here we showed that, within the arm bulk, a transmural strain gradient is present and have a functional relevance during muscle isotonic relaxation and cyclic sinusoidal length change representing natural cyclic movements. A nonuniform distribution of connective tissue fibers has been found also in other soft-bodied invertebrate muscle such as the squid mantle (Kurth et al., 2014). According to Kurth and colleagues, the organization of intra-muscular collagen fibers equalizes the nonuniformity in circumferential strain present during certain patterns of respiration and especially during the "hyper-inflation", a mantle expansion that anticipates a powerful escape jet.

This organization has also an interesting vertebrate-analogous in slow muscles, important for posture maintenance, and fast muscles, involved in rapid movements (Berne et al., 2010). Similarly, in the arm, inner muscle layers might function to accommodate strain and outer layers might work as elastic energy storage and release compartments. In support of this, we found differences in muscle activation properties (time to peak, force-frequency curve, twitch/tetanus ratio) wherefore outer layers manifest a kinetic of activation typical of skeletal fast-type muscle while inner layers show slow type properties. It would be tempting to speculate that these differences are determined by the presence of various forms of myosin or by a diverse mitochondrial volume density but, in the current state, these aspects deserve further investigations. Yet, it is worth notice that a metabolic differentiation was found across squid mantle muscles where the analogous of red and white fibers have been found at specific

location of the mantle thickness and thought to have a functional relevance during mantle deformations (Mommsen et al., 1981).

Taken together these findings open to another interesting question concerning the influence of muscle strain rate on mechanical work output. Muscle work loop shape, and so its relative *in vivo* function, varied depending on stimulation time. Inner and outer layers can act as motors thus generating energy (as the pigeon pectoralis muscle, figure 51a) or as brakes thus absorbing energy (as cockroach extensor muscle, figure 51b). We found that cyclic length changes coupled with phasic stimulation induced in all muscles the same work loop shape and net mechanical work, thus implicating that muscle optimal length was similar in outer and inner muscle layers. Studies in whole-organism locomotion in natural environments revealed that the nervous system can modulate mechanical performance setting the timing of activation of muscles. Examples can be found in fish axial muscles, that during swimming undulatory waves may play either a force-generating or a force-transmitting role and in turkeys gastrocnemius muscle that generates positive power during uphill running but acts as a strut during level running allowing tendon to store energy (figure 51c-d) (Dickinson et al., 2010; Rome, 2016).

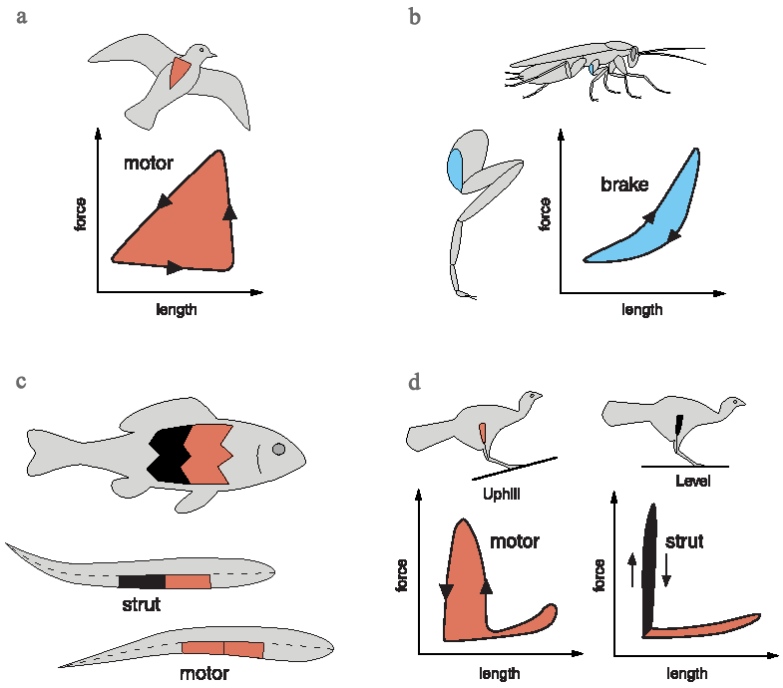

Figure 51: Muscle work loops and their functions. a) Pigeon pectoralis muscle generates the positive power to fly. b) Cockroach extensor muscle acts as a brake during running to slow the swing of the leg. c) Fish muscle function varies during swimming undulatory cycle. d) Turkey gastrocnemius muscle generates positive power during uphill running but acts as a strut during level running (adapted from Dickinson et al., 2010)

Similarly, in octopus whole arm movements the timing of muscle activation is crucial as a central motor input may reach outer and inner antagonistic muscles at different point of their shortening-lengthening cycles. This is particularly evident during arm elongation (figure 52) where these two muscle types are under different strain conditions.

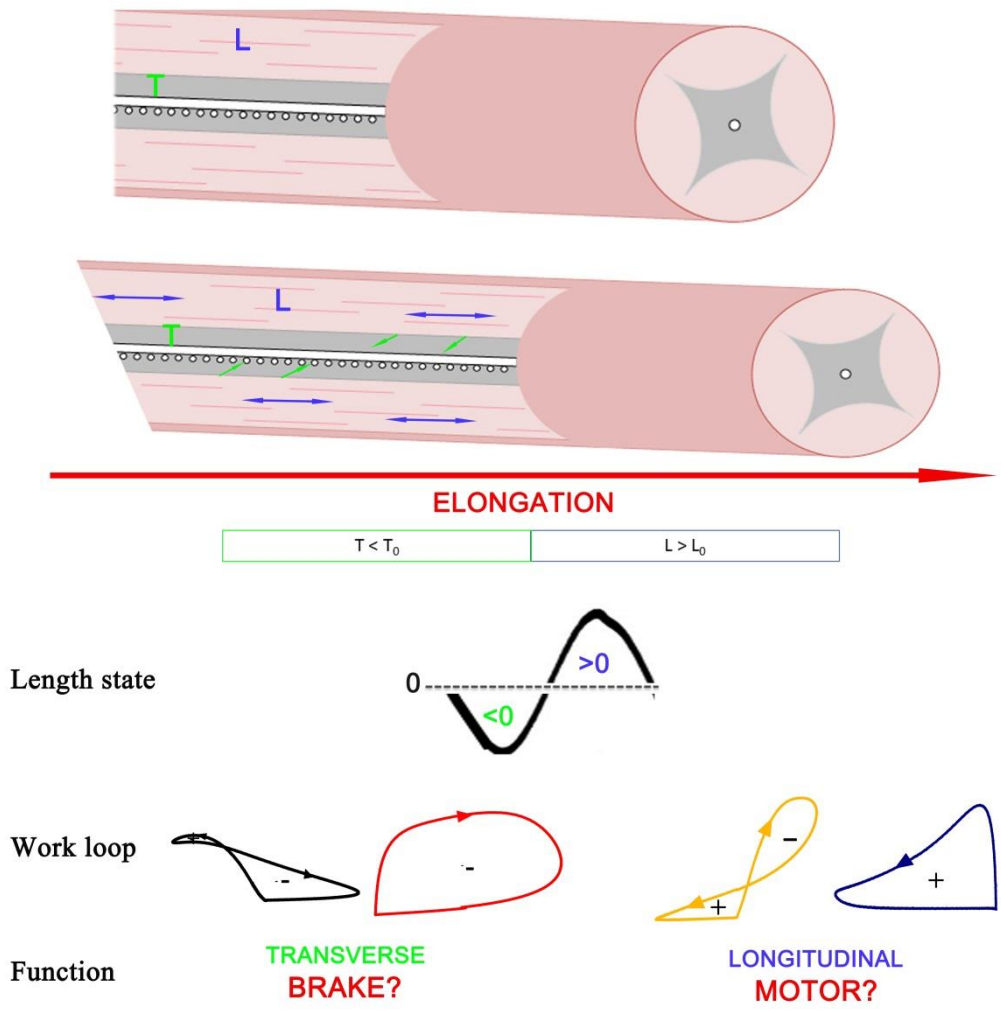

Figure 52: Possible *in vivo* functions of inner (transverse) and outer (lonitudinal) layers during octopus arm elongation. Transverse muscles may act as brake and longitudinal muscles as motors.

Given the low rate of innervation of a single arm muscle cell and the small area innervated by each motorneuron (Matzner et al, 2000; Nesher et al., *in prep.*), coordination of a large portion of muscles might not be an easy task. Here we show that a high level of coordination can be achieved locally between neighboring muscles exploiting the presence of unc-9-like functionally active gap junctions on the sarcolemma membrane. Interestingly a similar mechanism of coordination has been found in *C. elegans* in which gap junctions participate in the electrical coupling and coordination of body wall muscle cells during movements. Moreover, in *C. elegans* it has been suggested that the SR is nonessential for the excitation-contraction but might be important to enhance and orchestrate the animal body motility (Norman and Maricq, 2007).

Arm muscle coordination ability is also interesting in light of the excitation/contraction properties of single muscle cells. Here we showed that activation of contraction in muscle cells occurs in two ways, the first mediated mainly via direct activation of the contractile machinery by Ca^{2+} influx through the voltage-dependent Ca^{2+} channels and the second involving the recruitment of additional Ca^{2+} from internal stores in a Ca^{2+} dependent Ca^{2+} release mechanism (Nesher et al., in prep). These two modalities might be involved in different types of motion requiring for example either a fast and transient muscle contraction or a contraction sustained in time. This suggests that octopus arm muscles evolved together with a fine-tuned coordination and control mechanism where each muscle type might differently contribute to the overall arm performance. Taken together these studies convey the basic principles of hydrostatic limb flexibility and adaptability to a changing environment and point towards their relevance in a bio-robotic field.

6. Future perspectives

The octopus arm is one of the most versatile and performing structures built up by evolution. In this thesis, the octopus arm muscle structure-function relationship was investigated at the level of each muscle type. Several issues still need to be addressed and clarified with respect to the arm biomechanics and it would be necessary to investigate the entirely unexplored domain of biomechanics and dynamics of muscle contraction at the single cell scale. In particular, it would be important to assess if the difference in muscle activation kinetics is due to a specialization in the myofilament lattice proteins and in particular to the expression of specific myosin heavy chain isoforms. This aspect would be particularly useful for a further implementation of our biomechanical data in the 3 elements Hill's model.

This seemingly trivial aspect is particularly interesting when seen from a bio-robotic perspective as it can provide a useful mean to simulate the behavior of muscles as well as of artificial actuators varying the active and passive elements within the model until obtaining the desired performance. In addition, taking inspiration from the morphological composition of the arm muscles, it would be possible to develop various classes of soft actuators able to perform differently on the bases of their passive embedding and activation system.

7. Acknowledgments

I am grateful to my supervisor, dr. Letizia Zullo, whose kind advice, sincere curiosity, understanding and support pushed me further than I thought I could go.

I would like to thank dr. Anna Rocchi for her help and expertise.

I want to thank my colleagues and friends, Edu, Fede, Amanda and Ale, who indirectly helped me in completing my PhD.

Thanks to my family that shaped me into the determined person I am today and always kept me going.

Thanks to Andrea for his motivation, his belief in me and his patience. This journey would have not been possible without his unconditional support.

8. Bibliography

Abmayr, S. M., and G. K. Pavlath. 2012. “Myoblast Fusion: Lessons from Flies and Mice.” *Development* 139 (4): 641–56. doi:10.1242/dev.068353.

Altun, Zeynep F, Bojun Chen, Zhao-Weng Wang, and David H Hall. 2009. “High Resolution Map of Caenorhabditis Elegans Gap Junction Proteins.” *Developmental Dynamics : An Official Publication of the American Association of Anatomists* 238 (8). NIH Public Access: 1936–50. doi:10.1002/dvdy.22025.

Bairati, Aurelio, M. Comazzi, and M. Gioria. 2003. “An Ultrastructural Study of Connective Tissue in Mollusc Integument III Cephalopoda.” *Tissue and Cell* 35 (3): 155–68. doi:10.1016/S0040-8166(03)00017-X.

Bao, Guanjun, Hui Fang, Lingfeng Chen, Yuehua Wan, Fang Xu, Qinghua Yang, and Libin Zhang. 2018. “Soft Robotics: Academic Insights and Perspectives Through Bibliometric Analysis.” *Soft Robotics* 5 (3). Mary Ann Liebert, Inc.: 229–41. doi:10.1089/soro.2017.0135.

Bauer, Reinhard, Birgit Löer, Katinka Ostrowski, Julia Martini, Andy Weimbs, Hildegard Lechner, and Michael Hoch. 2005. “Intercellular Communication: The Drosophila Innexin Multiprotein Family of Gap Junction Proteins.” *Chemistry and Biology* 12 (5): 515–26. doi:10.1016/j.chembiol.2005.02.013.

Beckham, J David. 2016. “4EBP-Dependent Signaling Supports West Nile Virus,” no. November. doi:10.3390/v8100287.

Berne, Robert M., Bruce M. Koeppen, and Bruce A. Stanton. 2010. *Berne & Levy Physiology*. Mosby/Elsevier.

Bone, Q., E. R. Brown, and M. Usher. 1995. "The Structure and Physiology of Cephalopod Muscle Fibres." In *Cephalopod NeurobiologyNeuroscience Studies in Squid, Octopus and Cuttlefish*, 302–30. Oxford University Press. doi:10.1093/acprof:oso/9780198547907.003.0206.

Cianchetti, M., M. Calisti, L. Margheri, M. Kuba, and C. Laschi. 2015. "Bioinspired Locomotion and Grasping in Water: The Soft Eight-Arm OCTOPUS Robot." *Bioinspiration and Biomimetics* 10 (3). IOP Publishing. doi:10.1088/1748-3190/10/3/035003.

Corbetta, S., A. Bairati, and L. Vitellaro Zuccarello. 2002. "Immunohistochemical Study of Subepidermal Connective of Molluscan Integument." *European Journal of Histochemistry* 46 (3): 259–72.

Dickinson, Michael H, Michael H Dickinson, Claire T Farley, Robert J Full, M A R Koehl, Rodger Kram, and Steven Lehman. 2010. "How Animals Move : An Integrative View" 100 (2000). doi:10.1126/science.288.5463.100.

Farrell Peter, Joyner Michael and Caiozzo Vincent. 2006. *ACSM's Advanced Exercise Physiology*. Lippincott Williams & Wilkins.

Feinstein, N., N. Nesher, and B. Hochner. 2011. "Functional Morphology of the Neuromuscular System of the Octopus Vulgaris Arm." *Vie et Milieu* 61 (4): 219–29.

Fossati, S., F. Benfenati, and L. Zullo. 2011. "Morphological Characterization of the Octopus Vulgaris Arm." *Vie et Milieu* 61 (4): 191–95.

Full, Robert, and Kenneth Meijer. 2004. "Metrics of Natural Muscle Function." *Electroactive*

Polymer (EAP) Actuators as Artificial Muscles: Reality, Potential, and Challenges, Second Edition, 73–89. doi:10.1117/3.547465.ch3.

Gajardo-Gómez, Rosario, Valeria C. Labra, and Juan A. Orellana. 2016. "Connexins and Pannexins: New Insights into Microglial Functions and Dysfunctions." *Frontiers in Molecular Neuroscience* 9 (September): 1–19. doi:10.3389/fnmol.2016.00086.

Graziadei, P. 1965. "Muscle Receptors in Cephalopods." *Proceedings of the Royal Society of London B: Biological Sciences* 161 (984).

Hill, A. V. 1938. "The Heat of Shortening and the Dynamic Constants of Muscle." *Proceedings of the Royal Society B: Biological Sciences* 126 (843): 136–95. doi:10.1098/rspb.1938.0050.

Hochachka, Peter W. 1983. *The Mollusca. Volume 1, Metabolic Biochemistry and Molecular Biomechanics*.

Hooper, Scott L., Kevin H. Hobbs, and Jeffrey B. Thuma. 2008. "Invertebrate Muscles: Thin and Thick Filament Structure; Molecular Basis of Contraction and Its Regulation, Catch and Asynchronous Muscle." *Progress in Neurobiology* 86 (2): 72–127. doi:10.1016/j.pneurobio.2008.06.004.

Jospin, Maëlle, Vincent Jacquemond, Marie Christine Mariol, Laurent Ségalat, and Bruno Allard. 2002. "The L-Type Voltage-Dependent Ca2+channel EGL-19 Controls Body Wall Muscle Function in Caenorhabditis Elegans." *Journal of Cell Biology* 159 (2): 337–47. doi:10.1083/jcb.200203055.

Kier William M., Smith Kathleen K. 1985. "Tongues, Tentacles and Trunks: The Biomechanics of Movement in Muscular-Hydrostats." *Zoological Journal of the Linnean Society* 83: 307–24.

Kier, William M, and Nancy a Curtin. 2002. “Fast Muscle in Squid (Loligo Pealei): Contractile Properties of a Specialized Muscle Fibre Type.” *The Journal of Experimental Biology* 205: 1907–16.

Kier, William M, and Michael P Stella. 2007. “The Arrangement and Function of Octopus Arm Musculature and Connective Tissue.” *Journal of Morphology* 268 (10): 831–43. doi:10.1002/jmor.10548.

Kurth, Jessica A., Joseph T. Thompson, and William M. Kier. 2014. “Connective Tissue in Squid Mantle Is Arranged to Accommodate Strain Gradients.” *Biological Bulletin* 227 (1): 1–6.

Laplante, Mathieu, and David M Sabatini. 2012. “MTOR Signaling.” *Cold Spring Harbor Perspectives in Biology* 4 (2). Cold Spring Harbor Laboratory Press. doi:10.1101/cshperspect.a011593.

Laschi, C., B. Mazzolai, V. Mattoli, M. Cianchetti, and P. Dario. 2009. “Design of a Biomimetic Robotic Octopus Arm.” *Bioinspiration and Biomimetics* 4 (1). doi:10.1088/1748-3182/4/1/015006.

Laschi, Cecilia, and Matteo Cianchetti. 2014. “Soft Robotics: New Perspectives for Robot Bodyware and Control.” *Frontiers in Bioengineering and Biotechnology* 2. Frontiers Media SA: 3. doi:10.3389/fbioe.2014.00003.

Levy, Guy, Tamar Flash, and Binyamin Hochner. 2015. “Arm Coordination in Octopus Crawling Involves Unique Motor Control Strategies.” *Current Biology* 25 (9). Elsevier Ltd: 1195–1200. doi:10.1016/j.cub.2015.02.064.

Liu, Ping, Bojun Chen, and Zhao-Wen Wang. 2011. “Gap Junctions Synchronize Action Potentials and Ca $^{2+}$ Transients in *Caenorhabditis Elegans* Body Wall Muscle.” *Journal*

of Biological Chemistry 286 (51): 44285–93. doi:10.1074/jbc.M111.292078.

Liu, Qiang, Bojun Chen, Eric Gaier, Jaya Joshi, and Zhao-Wen Wang. 2006. "Low Conductance Gap Junctions Mediate Specific Electrical Coupling in Body-Wall Muscle Cells of *Caenorhabditis Elegans*." *Journal of Biological Chemistry* 281 (12): 7881–89. doi:10.1074/jbc.M512382200.

Lodish, Harvey F. 2000. *Molecular Cell Biology*. W.H. Freeman.

Lowey, J, B M Millman, and J Hanson. 1964. "Structure and Function in Smooth Tonic Muscles of Lamellibranch Molluscs." *Proceedings of the Royal Society of London. Series B, Biological Sciences* 160 (October): 525–36.

Mather, J. 1998. "How Do Octopuses Use Their Arms?" *J. Comparative Psychol.* 112 (3): 306–16.

Matzner, H, Y Gutfreund, and B Hochner. 2000. "Neuromuscular System of the Flexible Arm of the Octopus: Physiological Characterization." *Journal of Neurophysiology* 83 (3): 1315–28.

Milligan Brian J., Curtin N. A. and Bone Quentin. 1997. "Contractile Properties of Obliquely Striated Muscle from the Mantle of Squid (Alloteuthis Subulata) and Cuttlefish (Sepia Officinalis)." *The Journal of Experimental Biology* 200: 2425–36.

Mommsen, T. P., J. Ballantyne, D. Macdonald, J. Gosline, and P. W. Hochachka. 1981. "Analogues of Red and White Muscle in Squid Mantle." *Proceedings of the National Academy of Sciences* 78 (5): 3274–78. doi:10.1073/pnas.78.5.3274.

Morales, J., P. Montero, and A. Moral. 2000. "Isolation and Partial Characterization of Two Types of Muscle Collagen in Some Cephalopods." *Journal of Agricultural and Food Chemistry* 48 (6): 2142–48. doi:10.1021/jf990711k.

Motoyama, K., S. Ishizaki, Y. Nagashima, and K. Shiomi. 2006. “Cephalopod Tropomyosins: Identification as Major Allergens and Molecular Cloning.” *Food and Chemical Toxicology* 44 (12): 1997–2002. doi:10.1016/j.fct.2006.06.018.

Nesher N., Maiole F., Shomrat T., Hochner B., Zullo L. n.d. “The Neuromuscular Junction of the Octopus Arm Muscles.”

Norman, Kenneth R., and Andres Villu Maricq. 2007. “Innexin Function: Minding the Gap Junction.” *Current Biology* 17 (18): R812–14. doi:10.1016/j.cub.2007.07.043.

Oshima, Atsunori, Tomohiro Matsuzawa, Kouki Nishikawa, and Yoshinori Fujiyoshi. 2013. “Oligomeric Structure and Functional Characterization of Caenorhabditis Elegans Innexin-6 Gap Junction Protein.” *Journal of Biological Chemistry* 288 (15): 10513–21. doi:10.1074/jbc.M112.428383.

Pinotti I, Matheus Fécchio, Adriana Hepner Ii, Dijon Henrique, Salomé Campos, Leopoldo Muniz, Silva Iv, and Antonio Carlos. n.d. “Myocardial Contractility Impairment with Racemic Bupivacaine , Non-Racemic Bupivacaine and Ropivacaine . A Comparative Study 1” 30 (7): 484–90.

Raymond, Y. N.Lee, Leslie Lobel, Michael Hengartner, H. Robert Horvitz, and Leon Avery. 1997. “Mutations in the A1 Subunit of an L-Type Voltage-Activated Ca2+ Channel Cause Myotonia in Caenorhabditis Elegans.” *EMBO Journal* 16 (20): 6066–76. doi:10.1093/emboj/16.20.6066.

Rokni, Dan, and Binyamin Hochner. 2014. “Ionic Currents Underlying Fast Action Potentials in the Obliquely Striated Muscle Cells of the Octopus Arm Ionic Currents Underlying Fast Action Potentials in the Obliquely Striated Muscle Cells of the Octopus Arm,” 3386–97. doi:10.1152/jn.00383.2002.

Rome, Lawrence C. 2016. “The Effect of Temperature and Thermal Acclimation on the Sustainable Performance of Swimming Scup,” no. May 2007: 1995–2016. doi:10.1098/rstb.2007.2083.

Shaffer, Justin F, and William M Kier. 2012. “Muscular Tissues of the Squid Doryteuthis Pealeii Express Identical Myosin Heavy Chain Isoforms: An Alternative Mechanism for Tuning Contractile Speed.” *The Journal of Experimental Biology* 215: 239–46. doi:10.1242/jeb.064055.

Thompson, J. T., and W. M. Kier. 2001. “Ontogenetic Changes in Fibrous Connective Tissue Organization in the Oval Squid, Sepioteuthis Lessoniana Lesson, 1830.” *Biological Bulletin* 201 (2): 136–53. doi:10.2307/1543329.

Vogel, Benjamin, Hanna Siebert, Ulrich Hofmann, and Stefan Frantz. 2015. “Determination of Collagen Content within Picrosirius Red Stained Paraffin-Embedded Tissue Sections Using Fluorescence Microscopy.” *MethodsX* 2. Elsevier B.V.: 124–34. doi:10.1016/j.mex.2015.02.007.

Watson, Kurt, and Keith Baar. 2014. “MTOR and the Health Benefits of Exercise.” *Seminars in Cell and Developmental Biology* 36. Elsevier Ltd: 130–39. doi:10.1016/j.semcdb.2014.08.013.

Wood, William Barry. 1988. *The Nematode Caenorhabditis Elegans*. Cold Spring Harbor Laboratory.

Yen, Ming Ren, Milton H Saier, and Jr. 2007. “Gap Junctional Proteins of Animals: The Innexin/Pannexin Superfamily.” *Progress in Biophysics and Molecular Biology* 94 (1–2). NIH Public Access: 5–14. doi:10.1016/j.pbiomolbio.2007.03.006.

Zullo Letizia, Eichenstein Hadas, Federica Maiole, Hochner Binyamin. n.d. “Motor Control

Pathways in the Nervous System of the Octopus Vulgaris Arm."

Zullo Letizia, Sara M. Fossati, Pamela Imperadore, and Marie-Therese Nödl. 2017. "Molecular Determinants of Cephalopod Muscles and Their Implication in Muscle Regeneration." *Frontiers in Cell and Developmental Biology* 5 (May): 53. doi:10.3389/fcell.2017.00053.

9. Appendix

Articles in preparation/submitted during the PhD course

Zullo Letizia, Eichenstein Hadas, **Federica Maiole**, Hochner Binyamin

"Motor control pathways in the nervous system of the Octopus vulgaris arm" *(submitted)*

Nir Nesher, **Federica Maiole**, Tal Shomrat, Benyamin Hochner, Letizia Zullo

"The Neuromuscular Junction of the Octopus arm muscles" *(in preparation)*